Delft University of Technology

MASTERS THESIS
SET

Feasibility of using electric drone main rotors for electricity generation vs. solar panels for indefinite flight

Nicholas Dvorsky (4788214)
SUPERVISED BY:

Dr. ir. Michiel Zaaijer
Ir. Bart Remes
April 27, 2021

TU Delft Delft University of Technology

Acknowledgements

I would like to thank my supervisor Michiel for all of his flexibility, help, and guidance.

Thanks to Bart for providing the great idea for this project.

Thanks to my parents for the support that allowed me to pursue this education.

Thanks to old and new friends Jack, Ty, Bertram, Gabriel and others who helped make my time here enjoyable.

Abstract

An idea was proposed to allow an autonomous drone to have indefinite flight times over the ocean by applying renewable energy technologies and theory to generate electricity in flight. This is considered less as a way to save energy, but to permit the use of such a drone from a ship not capable of safely retrieving it. One novel component of this idea is to use the wind updraft created by the motion of a ship or natural air currents as the wind source for an on-board turbine generator. The second component is to use the existing drive system as the on-board turbine in a 'hybrid rotor' design to reduce the need for extra parts and complexity. This report analyzes the potential for such a system compared to a more intuitive airborne solar system, and to the combination of both concepts. While indefinite flight time is paramount, the goal is to maximize the "mission" time to charge/idle time ratio. The process for determining fitness is a simulation of the aircraft flying on its mission and charging when needed (and if possible) for a full year for varying designs of aircraft and rotor. The results of all the tests show that the main idea is infeasible because not enough energy can be generated from the inefficient propeller and the updrafts are insufficient and inconsistent. The alternatives of solar and combined power systems function better but are still subject to high failure rates. The most promising system is to use a separate turbine and propeller and also include solar panels to achieve the most effectiveness both when in powered flight and while charging. This constitutes a compromise on the 'hybrid rotor' part of the idea. The conclusion of this report is that further improvements to the design and control of the most successful configuration are possible could result in a fully functional system.

Contents

Abstract **2**

Nomenclature **4**

1 Introduction **6**
1.1 Background . . . 6
1.2 Project description . . . 9
1.3 Research questions and scope . . . 9

2 Methods **11**
2.1 Model Overview . . . 11
2.2 Solar Power Calculations . . . 13
2.3 Turbine Calculations . . . 13
2.3.1 Blade element momentum Theory . . . 13
2.3.2 Verifying rotor model accuracy . . . 17
2.4 Wind field calculations . . . 21
2.5 Aircraft performance calculations . . . 22
2.5.1 Glide speed . . . 22
2.5.2 Cruise Power . . . 22
2.5.3 Motor/Generator efficiency . . . 22
2.6 Implementation in code . . . 24

3 Mission simulations **26**
3.1 Case study description . . . 26
3.1.1 Design of the mission . . . 26
3.1.2 Aircraft design and control . . . 27
3.1.3 Rotor information . . . 29
3.1.4 Design of the experiments . . . 30
3.2 Baseline case and detailed performance explanation . . . 31
3.3 Independent ship and aircraft scenario . . . 34
3.3.1 Detailed tests . . . 35
3.3.2 Optimized test . . . 37
3.4 Cooperating ship and aircraft scenario . . . 39
3.4.1 Detailed tests . . . 39
3.4.2 Optimized test . . . 41
3.5 Separate turbine capabilities . . . 42

4 Discussion **44**
4.1 Deep dive in results . . . 44
4.2 Improvements to flight control and future research . . . 46
4.3 New ideas . . . 50

5 Conclusion and Recommendation **52**

Bibliography **54**

A Appendix: Motor specifications table **56**

Nomenclature

Abbreviations

2D	Two Dimensional
AWE	Airborne Wind Energy
BEM	Blade Element Momentum
CFD	Computational fluid dynamics
EQE	External Quantum Efficiency
GHI	Global Horizontal Irradiation
III-V	Three-five
LASER	Light Amplification by Stimulated Emission of Radiation
MAVLab	Micro Air Vehicle Laboratory
NLD	Never Landing Drone
PVGIS	Photovoltaic Geographic Information System
RPM	Rotations Per Minute
SOC	State of Charge
TMY	Typical Meteorological Year
TSR	Tip Speed Ratio
UAV	Unmanned Aerial Vehicle

Symbols

α	Local angle of attack	[Degrees]
η_{solar}	Solar energy conversion efficiency	
λ	Tip speed ratio	
Ω	Angular velocity	[rad/s]
ϕ	Inflow angle	[Degrees]
ρ	Density of air	[kg/m^3]
Θ	Rotor Pitch	[in]
θ	Local blade twist	[Degrees]
A	Airfoil wind section area	[m^2]
a	Induction factor	
A_e	Downstream area	[m^2]
A_o	Upstream area	[m^2]
B	Number of blades	
c	Blade chord	[m]
C_d	Coefficient of drag	
C_l	Coefficient of lift	
$C_{t,mt}$	Coefficient of thrust, Blade element theory	
$C_{t,mt}$	Coefficient of thrust, Momentum theory	
$C_{t,mt}$	Differential element torque coefficient	
D	Drag force	[N]
dA	Differential element of rotor area	[m^2]
dD	Differential element Lift	[N]
dF_n	Differential element normal force	[N]
dL	Differential element Lift	[N]
dr	Differential element of rotor radius	[m]
dT	Differential element tangential force	[N]
F	Tip loss correction factor	
F_n	Normal force	[N]
F_t	Tangential force	[N]
g	Gravitational constant	[m/s^2]
I	Current	[A]
i_o	No-load current	[A]
kV	kV	[$\frac{RPM}{V \cdot s}$]
L	Lift force	[N]
m	Mass flow rate	[kg/s]
$m_{aircraft}$	Mass of aircraft	[kg]
P_{copper}	Copper (ohmic) losses	[W]
P_{in}	Power in	[W]

P_{iron}	Iron losses	[W]	U	Upstream wind velocity	[m/s]
P_{out}	Power out	[W]	U_e	Downstream wind velocity	[m/s]
P_{solar}	Total solar power	$[W]$	U_g	Glide speed	[m/s]
r	Local radius of the rotor	[m]	U_r	Wind velocity at the rotor	[m/s]
R	Radius of the rotor	[m]	V	Voltage	[V]
R_m	Electrical resistance	[ohm]	V_{res}	Resultant velocity	[m/s]
R_{frac}	Fractional radius position		P	Power	$[W]$
S	Surface area of the 'wing'	$[m^2]$	T	Thrust	$[N]$

1 Introduction

This chapter contains background information and a current understanding of the subjects discussed in the rest of the report. This report and analysis is part of a larger collaborative project for the MAVLab so a description of other components and requirements of the project is also included. Finally, the research questions to be explored are stated.

1.1 Background

Drone aircraft are becoming an increasingly popular tool for performing useful work rather than just recreation as they have mobility and capabilities only found with aircraft and can be simpler and less restrictive than larger manned vehicles. In many cases, the work may require traveling long distances or simply staying airborne for extended periods of time. Attempts to build long range, endurance aircraft usually result in liquid fuel for it's high energy density, a large airframe designed for maximum efficiency, and naturally, the eventual need to land for refueling. Ultimately, the need to refuel is the limitation for all endurance aircraft. The use of fuel alone can present new problems as it can be explosive and a gas engine can have issues mid-flight due to its many moving parts. An alternative is electric aircraft but small electric aircraft are often greatly limited in range and operational time. Naturally, interested parties wish to investigate ways to improve the ratio of up-time to down-time for their working drones regardless of how they are powered.

In-air refueling is already used in some military aircraft to permit their planes to have an extended range. This can even improve efficiency such that the aircraft can have a greater range than a larger vehicle with the same fuel capacity [1]. However, this system suffers from the same issue of having a vehicle that needs to land which also exists entirely to support the main vehicle in addition to the issues of even greater mechanical complexity. Therefore, it is the field of renewable energy that some organizations are interested in because those principles and technology can allow for increased efficiency, and most importantly, power generation in flight. A self sufficient craft capable of indefinite powered flight would not be possible without a way of drawing its energy from the environment.

One such example would be Solar Impulse 1 and its successor Solar Impulse 2 shown in Figure 1, which are iterations of a proof of concept manned aircraft that theoretically never has to land. They manage this with a design that allows for a solar array large enough to charge the aircraft during the day such that it can continue to fly throughout the night. The fact that Solar Impulse aircraft had to carry a human passenger certainly affected their flight capabilities. A similar concept applied in an unmanned aerial vehicle (UAV) would be even more effective considering the lack of life support systems and other heavy components.

Figure 1: Image of solar impulse 2 on the ground [2].

There is a whole class of aircraft which draw their energy from the environment: gliders. Gliders usually operate by riding in thermals, columns of rising warm air, to gain speed and altitude to travel for long distances and long periods of time. However gliders are limited because thermal updrafts are usually a daytime occurrence making continuous flight through the night difficult.

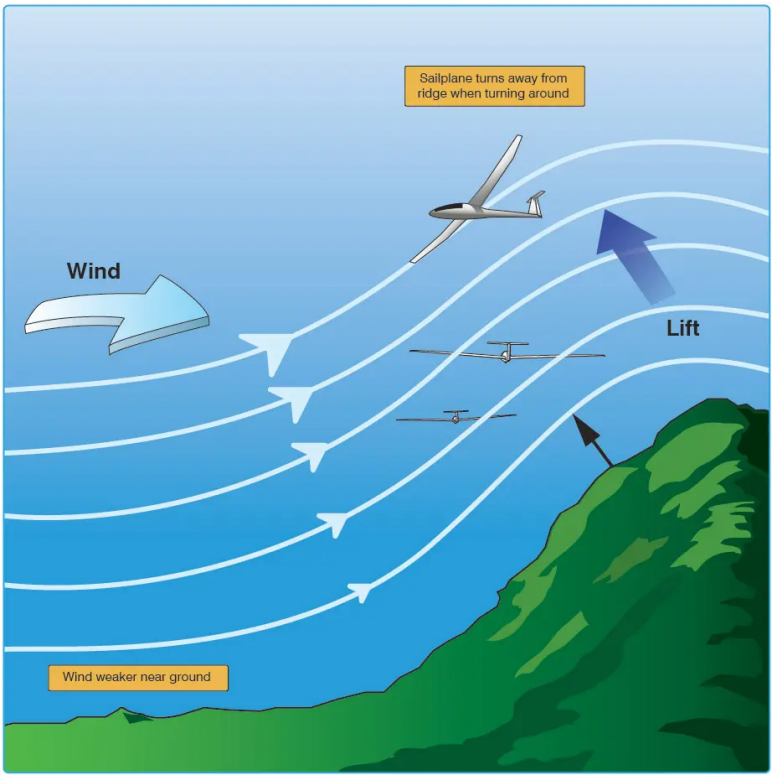

Figure 2: Diagram of the updraft effect of a hill and the basics of slope soaring [3].

Other sources of updrafts in the environment exist. When wind hits the base of a hill, its only option is to change direction to go up and over it (see Figure 2). These hills or cliffs introduce a vertical component to the wind that can be used by a glider. Unpowered flight in the updraft of a hill is called slope soaring and it can be sustained as long as there is continuous wind in the environment. A derivative of slope soaring is called dynamic soaring shown in Figure 3. Dynamic soaring extracts

energy from the change in wind speed between two nearby areas and can achieve speeds as high as 450 miles per hour [4]. This is done in the wind wake of a hill and has much greater energy potential than slope soaring. Regardless of their potential however, neither of these gliding techniques are possible without wind (and a hill) already being present.

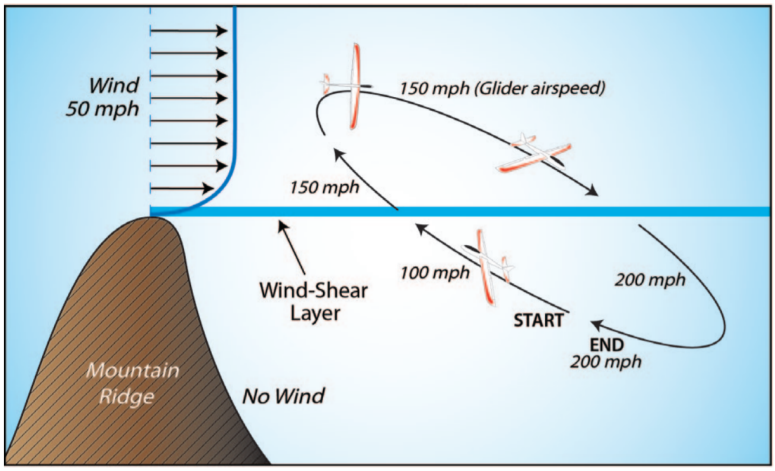

Figure 3: Diagram of the wind shear in the shadow of a ridge and the basic process of dynamic soaring [4].

Other entities seek to generate electricity in air for general use in national grids with specially designed flying turbines in the industry of airborne wind energy. Makani was one of the largest and most ambitious Airborne Wind Energy (AWE) companies and they used a system consisting of a tethered rigid wing aircraft with rotors that function both as motor-driven propellers for takeoff, and wind-driven generators once in flight [5]. The complete system is visible in Figure 4. This combination of typical flight hardware and the necessary components for extracting energy from wind into one system saves weight, reduces parts, and improves flight performance. However it does still require a non-conventional and more complex design for the combined unit. From their patent application, it seems that their rotors are asymmetrical indicating that they may be more optimized for either generation or forward thrust. They have patents indicating both fixed pitch and collective pitch which is another design variable which would have an effect on performance [6]. These solutions to the problem of multi-use hardware may not be worth the price for smaller projects or may still be too heavy from extra components. Further simplification may be needed for smaller aircraft.

Figure 4: Makani AWE system being tested over the ocean. It is in powered flight mode next to its base station at the time this picture was taken[7].

1.2 Project description

When a working drone has very limited access to landing zones, then reliable endurance can become particularly important. Flight over the ocean is treacherous because landing in the ocean rather than on land or a designated sea vessel would destroy most aircraft. Despite the difficulty, there are still applications for drone use over the ocean and the Dutch navy is interested in these applications and new solutions. The Micro Air Vehicle Laboratory (MAVLab) is attempting to develop what it calls the "Never Landing Drone" (NLD) for the Dutch navy; this project is part of that effort. The never landing drone is intended to allow aerial surveillance or search and rescue from ships that lack designated launch and landing space. This means that there is a limit to the maximum size of the NLD and the need to land must be minimized far beyond what is possible by conventional means. All of this is to be done without causing significant changes to existing navy operations and equipment. There are two main components that have defined and guided this project. First is the novel hardware and flight concepts created by the MAVLab that need to be developed from ideas into a framework that can be used in future designs. Secondly, the fitness of the concepts must be determined with respect to the desired mission of this drone to decide what potential future this idea may have. This section describes these in more detail.

The novel concept explored in this project is twofold. The MAVLab wishes to use the already present motor and propeller necessary for an electric aircraft, to generate electricity and recharge the on-board battery. This means using a common thrust optimized propeller that can be purchased at a store for the purpose of both propulsion and for generation of electricity as a wind turbine when conditions permit. The second novel component is the use of updrafts created by a moving ship as a way to keep a drone aloft and to provide it energy without landing. This would be a form of slope soaring that will be called static soaring which can be controlled and performed wherever desired. These concepts are compared and combined with a more intuitive source of mobile energy: solar panels. Both types of planes (wind and solar) will statically soar at the ship to reduce energy use when necessary. The ship has the option to turn into the wind to assist either type of aircraft by increasing the updraft but this is undesirable as it takes away the ability of the ship to perform its own mission.

Using a common propeller as the rotor for a wind turbine is certainly not as effective as a properly designed wind turbine rotor. Propellers are usually cambered and have an asymmetrical profile but when used as a turbine, the camber and profile will be reversed meaning the airfoil is inverted with respect to the direction of incoming air. Furthermore, the pitch of the blades for a propeller should be high for high speed travel but the pitch should be low for a wind turbine so it may rotate faster. The chosen airfoil is also different between the two types. These conflicts cast doubt on the usefulness of traditional rotor design, and what the optimal system will look like is unknown. The level of performance that can be expected from this hybrid rotor will determine the effectiveness of this concept for reducing mechanical complexity and weight.

Solar panels can easily be fitted onto an aircraft to provide some amount of electricity. This has already been done to some degree as mentioned above so it is acting as a reference against which the above concept will be compared. Because the behavior of solar panels is well-understood, it is easy to predict the performance of such a system. However, solar panels and the required electrical equipment will add weight and potential points of failure to the airframe and part of the purpose of this project is to investigate low-mechanical-complexity options.

1.3 Research questions and scope

This project is framed around determining the feasibility of the hardware within the scope of a non-specific mission. The mission in this case is to be launched at sea, fly some distance away from the ship it is launched from (the mothership) and to return to the mothership to charge or when battery level is low. Specific tasks for the drone to perform while on mission are outside the scope of this project but could include surveillance, imaging/mapping, search and rescue, etc. It is important for the strategies and technologies analyzed in this project to be optimized to maximize the amount of time spent on mission and minimize time spent at the mothership.

As this project is a collaboration some parts have been or will be developed by other researchers. In this part of the project, the ability to maintain proper positioning within the updraft of the ship is considered a given. Another researcher was responsible for developing the model of the updrafts caused by the ship and this report assumes that it is accurate. Additionally, the finer dynamics of flight on the mission are not considered.

With the limitations known, discovering whether the concept of a "never landing drone" is feasible in this preliminary study, can be done by answering the following questions:

- What is the effectiveness of using a propeller for a wind turbine rotor?
- How do changes in the hybrid rotor design affect performance as a complete system?
- What are motor and generator requirements and their effect on performance?
- What factors in the airframe design affect charging capability and mission performance?
- Can solar energy sustain an aircraft on this mission indefinitely?
- Is the novel wind powered, hybrid rotor approach better than alternatives (solar)?
- Can the drone operate without negatively affecting the mothership?

2 Methods

This chapter includes and describes the processes and models used for this project starting with an overview. After the overview is an explanation of the solar model followed by the process for calculating and then verifying rotor performance. Following the two generation methods are the calculations for how the aircraft will perform in the simulations. Finally, a description of the model for the wind field around the ship is given followed by an explanation of how these parts are brought together in the simulation program.

2.1 Model Overview

An overview of the entire process is useful to aid in understanding the more detailed components and how they work together. Figure 5 is a flowchart showing the critical steps of the calculations with an accompanying text description in the following paragraphs.

The simulation of the drone's performance used for these analyses is based on knowing the amount of energy that can be extracted at local conditions. For the solar drone, data recorded from weather monitoring satellites is used to inform the simulation of the amount of solar energy available at any time. For the hybrid rotor aircraft configuration the performance of the rotor as a propeller and a turbine must be calculated for the expected range of air speeds. This is done with BEM (Blade Element Momentum) theory commonly used for wind turbines.

In addition to knowing how much energy can be generated, a process for determining *when* energy can be generated to sustain or charge the system is needed. The solar aircraft can generate electricity as long as the sun is up so no extra effort needed to be applied there. To find when and how much electricity could be generated by the turbine, this report uses a model created by another researcher of the same larger project. That model receives the upstream relative wind velocity and aircraft parameters, to calculate where, within the disturbed air around the ship, the aircraft could statically soar and how much additional drag the turbine could be allowed to apply. This information and the results of the turbine design calculations has to be carefully matched by wind speed and thrust/drag so that the correct value of power can be found.

With the power generating aspects covered, the simulations also require the performance characteristics of the aircraft itself. These depend on the design of the rotor, the electronics, and also the design of the airframe. The cruise power affects how long the aircraft can stay on a mission and the glide speed determines when wind conditions permit soaring (and charging) at the ship.

With all the static performance calculations done the simulations can then be run using the different generation methods and operational modes. The process of the analysis progresses through a 1 year simulation of the aircraft, wind data, and ship "patrols" while checking at each time step if the aircraft is at the ship and able to charge, on mission, or drained of energy. The result of the simulations include the distribution of what the aircraft spent its time doing, the history of its charging rate, and its power draw. Analysis of what design choices are most effective for the overall system can then be performed on these results.

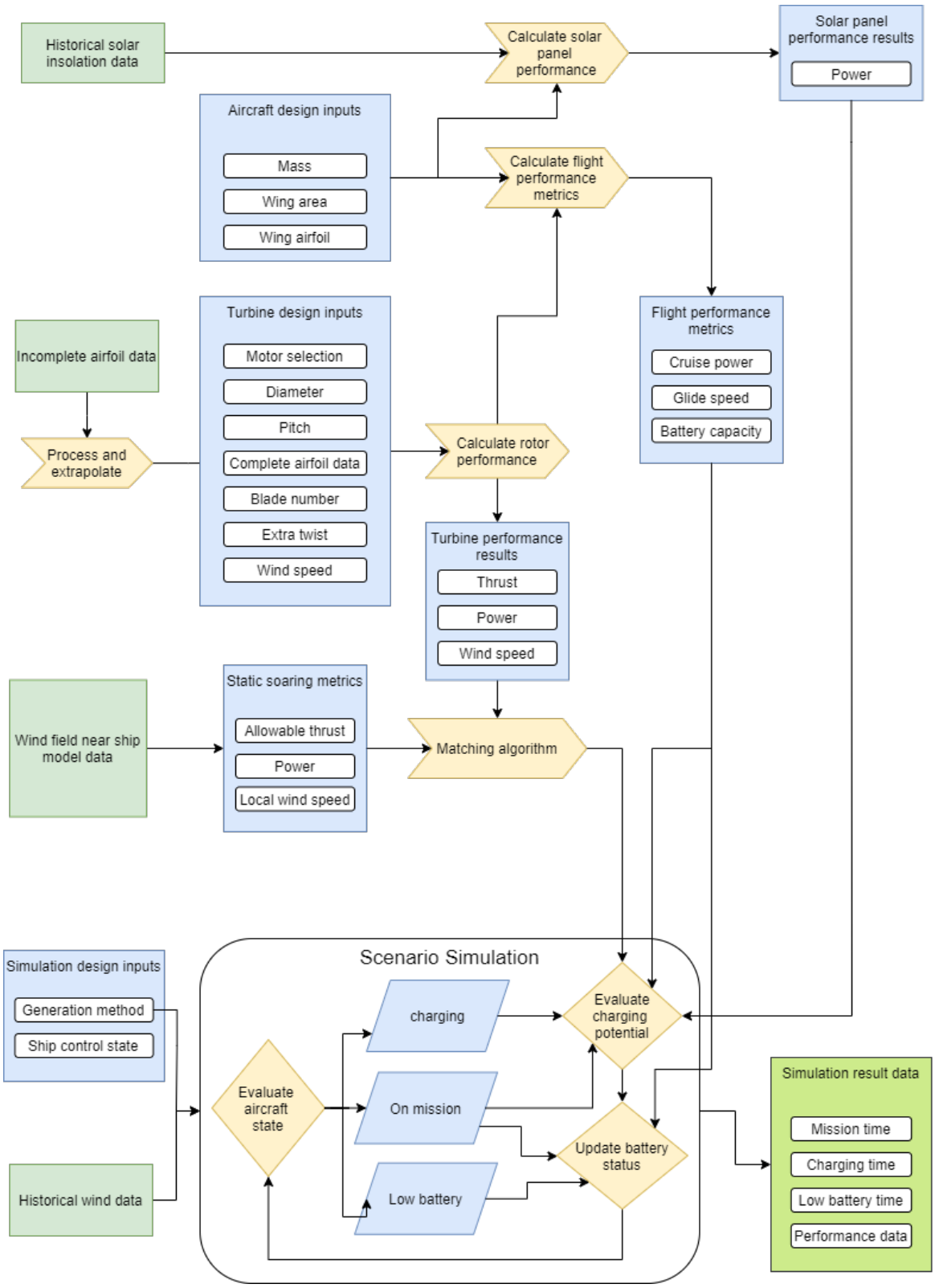

Figure 5: Flowchart showing the use of all calculations and the processes of the simulation.

2.2 Solar Power Calculations

The solar irradiance available to the solar panels was taken from historical satellite data. The movement of the Earth is regular and stable which allows predictive equations to model the amount of solar energy irradiating an area but this does not take into account atmospheric effects. Therefore, historical data is better as it is affected by the real weather where it was recorded.

The data used was collected from the European Commission's Photovoltaic Geographic Information System (PVGIS) website which contains data collected by satellites and processed by algorithms into local irradiation [8]. This is not as good as a direct measurement from a meteorological station but it has the advantage of providing data for almost any desired location. The data set chosen is from the TMY database which stands for Typical Meteorological Year which is meant to be representative of the normal climate of an area without any exceptional variations.

The most logical area on an aircraft to place solar cells is on its wings which are large, relatively flat surfaces. The wings of the aircraft are assumed to be horizontal at all times because time spent gaining or losing altitude and turning where the wings would be at an angle is insignificant. With horizontal surfaces the heading of the drone also has no impact on irradiation. For these reasons this analysis uses global horizontal irradiation (GHI) for the base solar model. GHI is a measure of the amount of solar energy that hits a horizontal surface per square meter of that surface.

The efficiency of solar panels (η) can be a wide range of values typically between 10 and 40%. The power produced by the solar panels (P_{solar}) at any time is a simple relationship shown in Equation 1 where S is the wing/solar area.

$$P_{solar} = \eta \cdot S \cdot GHI \tag{1}$$

2.3 Turbine Calculations

In this section, the theory used to calculate and predict the rotor's performance is described. Blade Element Momentum (BEM) theory is used for this and has many variations. The critical information for the version used in this project can be found in Equation 17, Equation 19, and Equation 20. After BEM theory, the verification process for the rotor calculations is presented.

2.3.1 Blade element momentum Theory

For the calculation of the performance of the rotor, Blade Element Momentum (BEM) theory for wind turbines is used. BEM theory makes no assumptions about whether the rotor in question is designed as a propeller or a turbine and propeller design also uses BEM theory [9] so no errors are expected on that account. There are slight differences mainly centering on what conventions define as positive [10]. It is for this reason that calculations based on BEM theory are assumed to be sufficient for evaluating the complete range of rotor performance in this project.

BEM theory begins with several common assumptions about the flow. It is assumed that the flow is inviscid, incompressible, without rotation, and that it is uniform across the rotor area [11]. Some of these assumptions can be replaced with additional models of flow but that is not done in this preliminary analysis.

Momentum theory is the first part of BEM and has several additional assumptions. The rotor will have the potential to interact with a column of air of the same diameter as itself but if it removes energy from the air flowing through it then it must have an effect on the column of air. To extract energy, the rotor will apply a thrust force T opposite to the direction of flow. This force will slow down the incoming air but considering the assumption that the air is incompressible, the crossectional area of the flow must change. This 'tube' of fluid, known as the stream tube is depicted in Figure 6.

Because no mass is lost in the process the conservation of mass can be applied to give Equation 2:

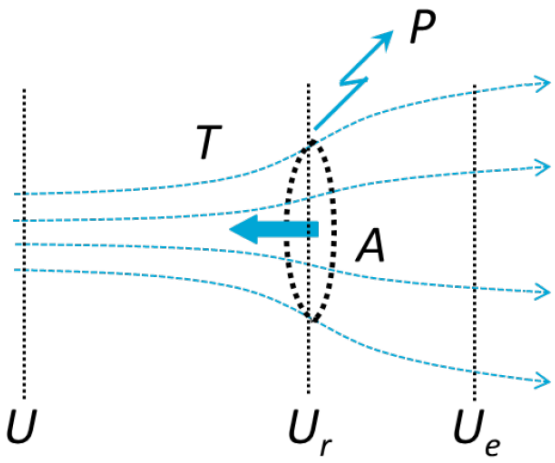

Figure 6: Visual depiction of rotor's effect on a column of air or "stream tube"[11].

$$A_o \cdot U = A_e \cdot U_e \tag{2}$$

which relates the area and velocity of the flow in the stream tube before and after the rotor. U is the [known] upstream velocity, U_e is the downstream velocity and A_o and A_e are the upstream and downstream areas respectively. Knowing how the velocity of the flow changes allows us to create an equation for the thrust force and the power as shown in equations Equation 3 and Equation 4:

$$T = m \cdot (U - U_e) \tag{3}$$

$$P = m \cdot (U - U_e) \cdot U_r \tag{4}$$

where U_r is the velocity at the rotor which is unknown. T and P are thrust and power respectively and m is the mass flow rate through the stream tube. These equations lack a way to calculate the thrust provided by the rotor because there are still unknown quantities (U_e and U_r). Blade Element theory uses the aerodynamics of the blades to help determine the effect they have on the airflow. To describe the different components of the air velocity around a section of the blade , known as a blade element, the velocity triangle which can be seen in Figure 7 is used.

The velocity triangle shows how the relationship between wind speed and the rotation of the rotor creates the inflow angle, and how the twist of the blade relates the inflow angle to the angle of attack of the blade airfoil. A key difference between wind turbine design and propeller design is that on the velocity triangle, the angle of attack becomes negative meaning the orientation of the airfoil is reversed to change in which direction the lift is produced. The Propeller oriented airfoil is drawn on the velocity triangle figure in red.

As seen in the figure, part of the relative wind velocity is a result of the rotation of the blade itself and is represented as $\Omega \cdot r$. Orthogonal to the rotation of the rotor is the incoming wind speed at the rotor U_r. The addition of these two vectors is called the resultant velocity which will be used in the calculation of aerodynamic forces on the blade. The inflow angle is the angle between the resultant velocity and the plane of rotation and is calculated as in Equation 5.

$$\phi = atan(\frac{U_r}{\Omega \cdot r}) \tag{5}$$

Because a component of the resultant wind velocity is determined by the tangential speed of the blade elements, and thus the radial position along the blade, a correction known as blade twist is introduced

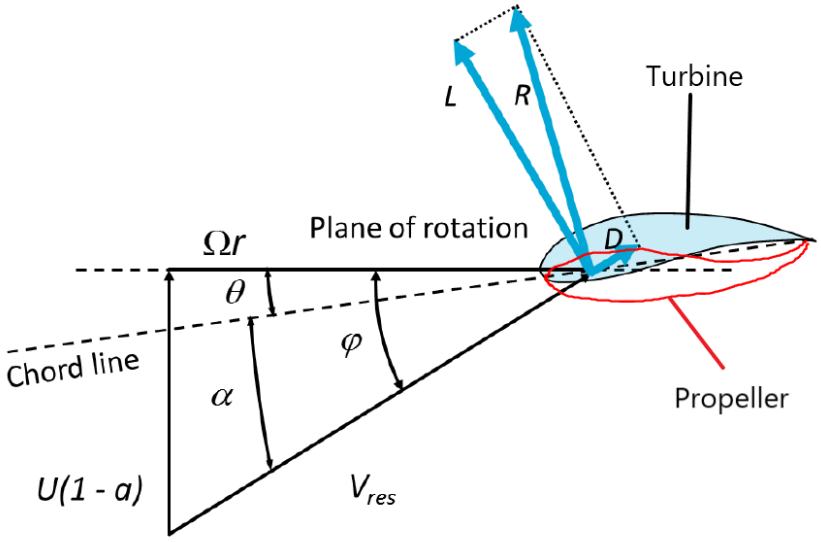

Figure 7: Velocity triangle of a wind turbine blade element with propeller airfoil alternate orientation drawn in red.

to maintain a desirable angle of attack and compensate for the changing inflow angle. The blade twist is represented by θ. Blade twist is the angle between the chord line of the airfoil and the plane of rotation. This means that the angle of attack of the resultant wind on the airfoil of the blade can then be calculated as in Equation 6.

$$\alpha = \phi - \theta \tag{6}$$

The aerodynamic forces lift and drag are defined in relation to the resultant velocity vector, but for the calculation of the performance of the rotor the forces tangent to the plane of rotation F_t and normal to the plane of rotation F_n are necessary. Fortunately they are related by the inflow angle and can be calculated using Equations 7 & 8.

$$F_n = L \cdot cos(\phi) + D \cdot sin(\phi) \tag{7}$$

$$F_t = L \cdot sin(\phi) - D \cdot cos(\Phi) \tag{8}$$

In Equation 7 and Equation 8, the letters 'L' and 'D' refer to lift and drag respectively which can be calculated in general form as:

$$L = \frac{1}{2} \cdot C_l \cdot \rho \cdot A \cdot U^2 \tag{9}$$

$$D = \frac{1}{2} \cdot C_d \cdot \rho \cdot A \cdot U^2 \tag{10}$$

where C_l and C_d are the lift and drag coefficients, ρ is the fluid density, A is the planform area of the aerodynamic surface and V is the fluid velocity. Lift and drag coefficients used here will vary with airfoil design and Reynolds number so they must also be altered to fit the current conditions on the blades. The ability to do this depends on the airfoil data source.

Blade element theory, as the name suggests, is a discrete element calculation. This is because the velocity experienced by the blades and the geometry of the blades themselves changes continuously

along their length. The changing conditions prevent the use of a single equation to calculate the performance of the rotor as a whole. Therefore, the equations must be re-written into element forms. The element forms for lift and drag are Equation 11 and Equation 12 respectively.

$$dL = \frac{1}{2} \cdot C_l \cdot \rho \cdot V_{res}^2 \cdot c \cdot dr \tag{11}$$

$$dD = \frac{1}{2} \cdot C_d \cdot \rho \cdot V_{res}^2 \cdot c \cdot dr \tag{12}$$

Here, the chord 'c' multiplied by the element size along the radial direction 'dr', stands in for the area of the small wing section being analyzed at the time. Additionally, the velocity term has changed as the blades experience an airspeed that is a combination of their angular velocity, position along the blades, and upstream wind speed. The relationship between the airspeed experienced by the blades and the upstream airspeed is given by Equation 13 where 'a' is the induction factor as defined in Equation 14.

$$V_{res} = \frac{U \cdot (1 - a)}{sin(\phi)} \tag{13}$$

$$a = \frac{U - U_r}{U} \tag{14}$$

By combining equations Equation 7, Equation 11, and Equation 12 the element equation for the normal force on the rotor plane is formed. Adding B, the blade number, to the equation accounts for the fact that there are multiple blades in the complete rotor.

$$dF_n = \frac{1}{2} \cdot B \cdot \rho \cdot V_{res}^2 \cdot c \cdot (C_l \cdot cos(\phi) + C_d \cdot sin(\phi)) \cdot dr \tag{15}$$

A similar equation exists for momentum theory which has been formed to calculate based on discrete rotor annuli. By performing the calculations over annuli, the results of the momentum theory equation can be directly related to the results of the blade element equation. The momentum theory thrust equation is Equation 16,

$$dT = \frac{1}{2} \cdot F \cdot \rho \cdot U^2 \cdot 2 \cdot \pi \cdot r \cdot dr \cdot 4 \cdot a \cdot (1 - a) \tag{16}$$

Due to the way lift is generated, the tips of wings, or in this case rotor blades, tend to form vortexes where air from below the blade flows around the tip to the upper part of the blade. F is the tip loss factor which is given by Equation 17 and is used to account for this behavior at the tips of the blades [9]. This must be included in the momentum theory equation because it pertains to the movement of air across radial segments of the rotor.

$$F = \frac{2}{\pi} \cdot acos(e^{\frac{-B}{2} \cdot \frac{1 - R_{frac}}{R_{frac} \cdot sin(|\phi|)}}) \tag{17}$$

Setting equations Equation 15 and Equation 16 equal to each other allows for an iterative process in which the unknown velocities are changed by adjusting the induction factor until a solution converges. To simplify the calculations however, these equations can change into their non-dimensional thrust coefficient forms. To do this, both equations will be divided by $\frac{1}{2} \cdot \rho \cdot U^2 \cdot A$ which is modified with Equation 18 to use an approximation of the area for small elements. The results, after some algebra, are Equation 19 and Equation 20 the former including the tip loss correction factor mentioned above.

$$A \approx 2 \cdot \pi \cdot r \cdot dr \tag{18}$$

$$C_{t,mt} = 4 \cdot a \cdot (1 - a) \cdot F \tag{19}$$

$$C_{t,be} = \frac{B \cdot c}{2 \cdot \pi \cdot r} \cdot (1 - a)^2 \cdot \frac{(C_l \cdot cos(\phi) + C_d \cdot sin(\phi))}{sin(\phi)^2} \tag{20}$$

Once the results of the two equations converge then the solution for the correct induction factor has been found. With this information the power can then be calculated. The discrete element coefficient of torque dCQ can be found using Equation 21 which can then be used in Equation 22 to calculate the total power.

$$dCQ = \frac{B \cdot c}{2 \cdot \pi \cdot r} \cdot Rfrac \cdot (C_l \cdot sin(\phi) - C_d \cdot cos(\phi)) \frac{(1 - a)^2}{sin(\phi)^2} \tag{21}$$

$$P = \sum dCQ \cdot \lambda \cdot \frac{1}{4} \cdot \rho \cdot U^3 \cdot dA \cdot \pi \tag{22}$$

λ is a ratio known as the Tip Speed Ratio (TSR) which is used in many of the plots throughout the report. It is the relationship between the speed of the tip of the rotor and the speed of the incoming wind as it rotates and is shown in Equation 23.

$$\lambda = \frac{\Omega \cdot R}{U} \tag{23}$$

2.3.2 Verifying rotor model accuracy

The results of the rotor calculations must be verified as they are not immediately recognizable as correct because the airfoil being designed backwards for a turbine results in unusual behavior. Several methods of verification were used.

For a propeller operated as a turbine, the results from the program do not match what was expected. When using a propeller as a wind turbine, there is a large region of low tip speed ratios which result in negative power generated. This can be seen in Figure 8. However, when the specified airfoil is replaced with any symmetrical airfoil (in this case ea61012) this region largely disappears and when running it with the original NACA 4412 airfoil, but with it oriented in the correct direction for turbine operation, the power-lambda curve is more like the shape that would be expected. Additionally, the turbine-oriented NACA 4412 airfoil outperforms the symmetrical airfoil when generating because it is optimized to produce higher lift in this orientation. Comparing the peak power generation of the properly (turbine) oriented airfoil to the thrust oriented airfoil (propeller) shows a difference of a factor of around 3x. Low performance was expected for the propeller acting as a wind turbine so this is unsurprising.

Investigating the source of the negative power region resulted in the conclusion that it was caused by drag. With the airfoil in an incorrect orientation, it produces significant drag (shown in Figure 9) until a higher rotor speed improves the angle of attack of the relative wind velocity on the blade. Additionally, the tip speed ratio where the drag coefficient reaches a relatively constant low value is the same as the point where it begins acting as a propeller rather than a turbine. This makes sense as the rotor in this case is designed to operate as a propeller so it should have the lowest aerodynamic drag in that state.

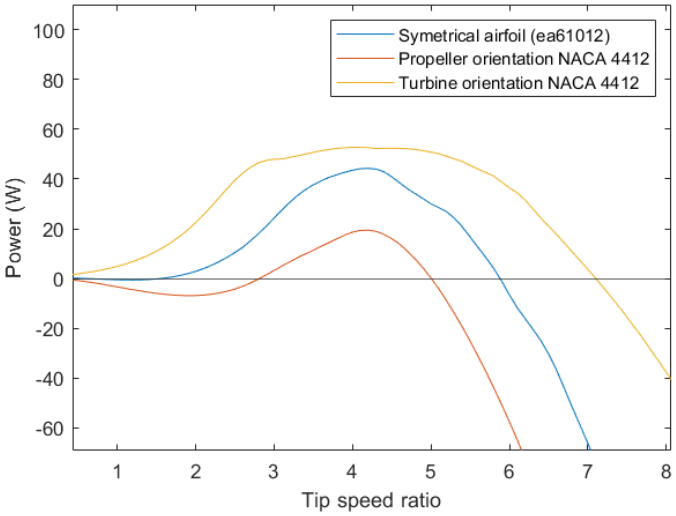

Figure 8: Direct comparison of generator power between different airfoils or airfoil orientations.

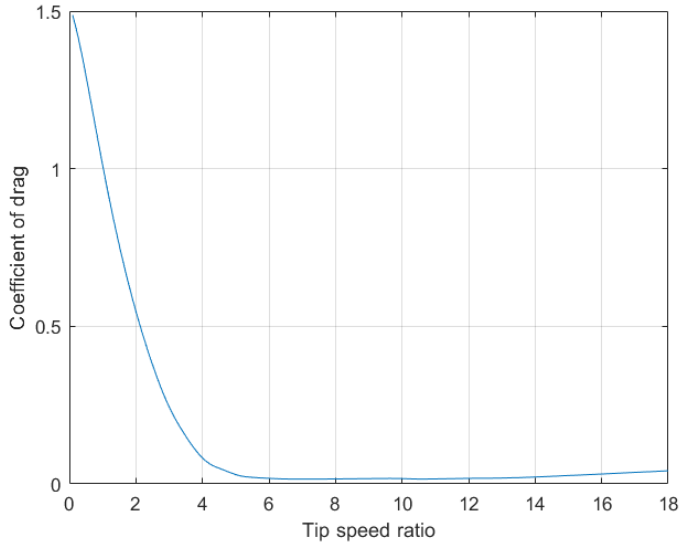

Figure 9: Coefficient of drag for a propeller shown across a range of tip speed ratios. This shows the high drag in the low speed 'turbine' region.

One method of verification that was considered was a comparison between the calculation results and data published by the company APC who manufactures some of the propellers used in the MAVLab. Their propeller is also the model which the chord is based on for all of the rotor designs tested as part of this project. Because part of the goal of this project is to model the performance of commonly available components, comparing the calculations to published data is ideal. APC states that their airfoils are based off of the NACA 4412 airfoil [12] and then modified slightly. For this reason, that airfoil is what was used throughout the project. However, once the calculations were compared to the manufacturer data, significant differences were found which could not be consistently corrected by an offset in the design inputs. Figure 10 shows on the left both the performance of an actual APC rotor as published by the company [12], and the results of the model for the same parameters, and it can easily be seen how they diverge. On the right side plot, the percent difference between the APC data and the calculated results is shown both if you are examining the change in thrust at the same RPM, or the difference in RPM if you are needing a certain thrust value. Additionally, as APC only produces *propellers*, they do not test them or supply data for them when operating as a wind turbine so no

comparison could be made to verify the performance of the model in that operational state.

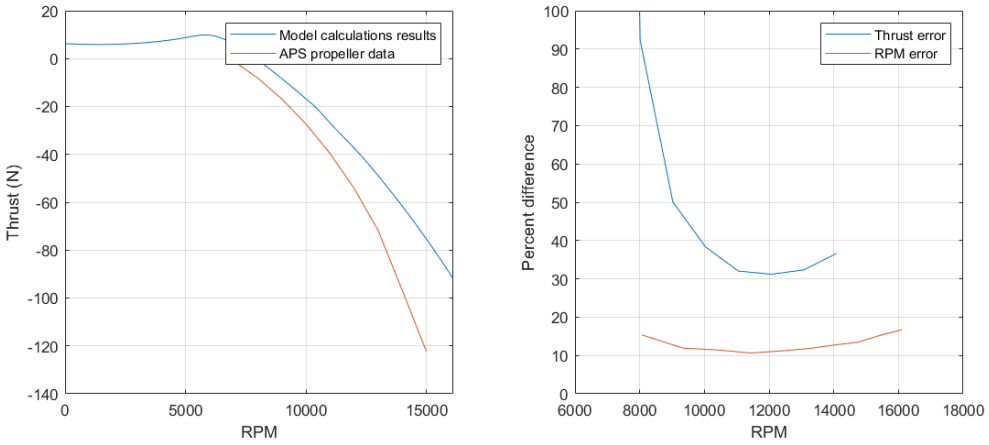

Figure 10: Comparison between APC published propeller performance data and the results of this model. Both for a rotor of 14in diameter and 7in pitch.

There are only two specifications given for commonly available propellers: diameter and pitch. These are commonly written in the format of the diameter in inches followed by 'x' and then the pitch, also in inches. Knowing that the company likely does not follow these values exactly in the real design, some variations were performed to search for a constant offset or consistent difference between the results of the given inputs and the data released by the company. For a larger rotor which is labeled 14x7, changing the pitch to 8.5 resulted in the average difference in the thrust results shown in Figure 11 falling below 5%. This was considered a good match. However, when altering the pitch of the other propeller designs, both by a constant offset of 1.5 inches or a change proportional to the difference in diameter, the other configurations did not improve. Some even required the change to be performed in the opposite direction to increase similarity between the respective calculations and specifications. The model should produce results which either match the manufacturer's data or have some predictable difference such that the difference can be corrected. If the specifications do not match perfectly with the actual design of the propellers then they cannot be depended on. Ultimately, not enough is known about the physical design of the propellers due to vague and incomplete information from the manufacturer. Because of the inconsistency in the comparisons, the APC performance data was abandoned as a method to verify the rotor calculations.

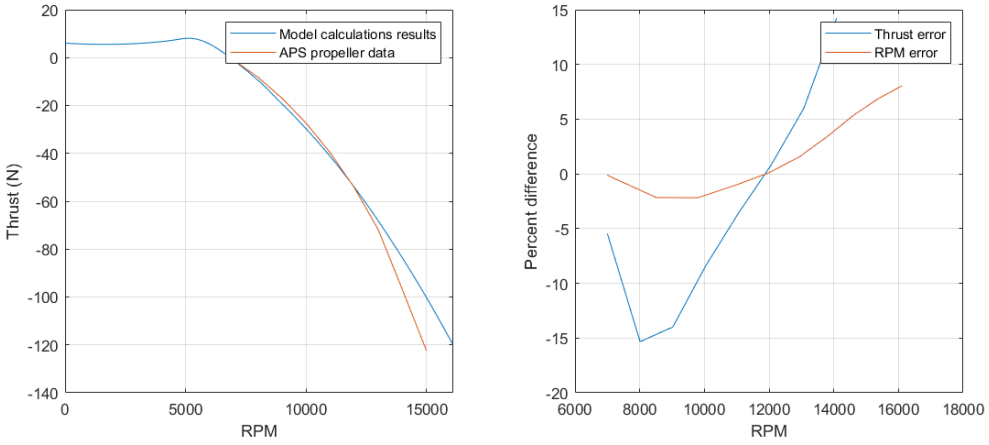

Figure 11: Comparison between APC published propeller performance data and the results of this model. APC rotor is 14in diameter and 7in pitch with the computer model results having changed the pitch to 8.5in. This shows better similarity.

Without the ability to compare the results of the rotor model to real data, only custom propellers or

those which can be carefully measured and replicated can be analyzed and compared with this model. In this report, partially custom propellers are used with only the chord being measured from actual products and the airfoil still following what is claimed by the manufacturer.

The second method of verification is to compare the results of the calculations to a different known and trusted source which could more easily be matched. In this case, the FASTTool simulation of the NREL 5MW turbine became the standard to compare against. FASTTool is provided by TU Delft. Within the FASTTool interface, the exact airfoil, diameter, blade twist, chord, and operating conditions can be chosen such that the model in this report can match them with more certainty than with the APC data.

Some modifications had to be made to the rotor design being compared because some of the airfoils were not available from the same source as all other airfoils used in this project. To this end, the blade airfoil design changed to the values listed in Table 1. These same values were used in the implemented model along with an exact copy of the twist and chord distributions and fine pitch angle. The comparison of power coefficient plotted against tip speed ratio λ is shown in Figure 12. One difference is unavoidable as FASTTool is not designed to use a variable Reynolds number whereas the current model is. This and the accompanying change in the lift and drag values along the blade is the cause for the slight difference. Regardless of slight differences, this test showed that there were no structural errors in the model and that the results will agree with the mainstream rotor theory.

Radial Position (m)	Airfoil
0 - 6.6	Cylinder 1
6.6 - 9.3	Cylinder 2
9.3 - 63	NACA 643618

Table 1: Blade and airfoil distribution of modified NREL 5MW design.

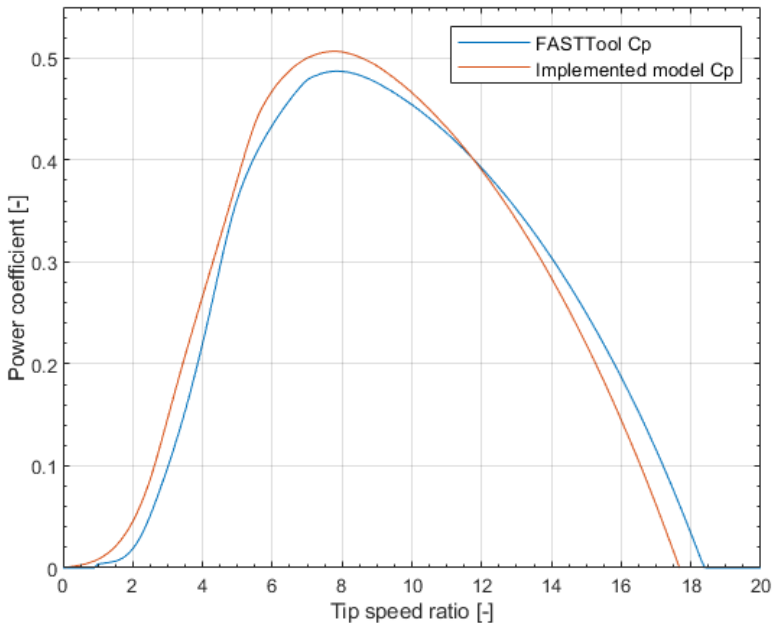

Figure 12: Direct comparison of power coefficient values calculated by the implemented model and by the FASTTool at the rated wind speed of 11 m/s.

2.4 Wind field calculations

An important prerequisite for simulating the completed aircraft is knowing the behavior of the environment it will be in. As this project is done as part of a larger collaborative effort, the interaction between the air and the moving ship, which produces the updrafts that sustain the aircraft, has been prepared by another researcher. A simple description of that process is as follows. Everything described in this subsection was created by and detailed in a pending report by Midas Gossye [13].

First, a simplified CFD solver determines the wind speed and direction for points around the obstruction (the mothership). This is done as a 2D analysis over a vertical, flat plane that bisects the ship. The solver is designed to trade some accuracy for speed as part of its purpose is to be able to run in real-time on board the aircraft to inform its guidance system. An example of the result of this program is shown graphically in Figure 13. This figure shows the streamlines of the flow in blue, the turbine thrust (drag) in shades of red and the direction and velocity of the disturbed wind field with a vector field in shades of purple. This plot is shown as an example of an early result and later versions of the program did not produce these plots. Though the performance of the guidance system is outside the scope of this project, use of the potential flow solver is still a required component from the larger collaboration as it will be running on the aircraft and will inform its guidance system when that gets developed. The ship, pictured in a side-view, is approximated as a quarter circle or oval at this stage of the overall project, and can be seen in the bottom left corner of the figure. The actual size of the ship can be altered within the wind field program to match whatever vessel is being used. The program requires only an upstream relative (to the ship) wind speed and the size of the ship to calculate the characteristics of the wind field.

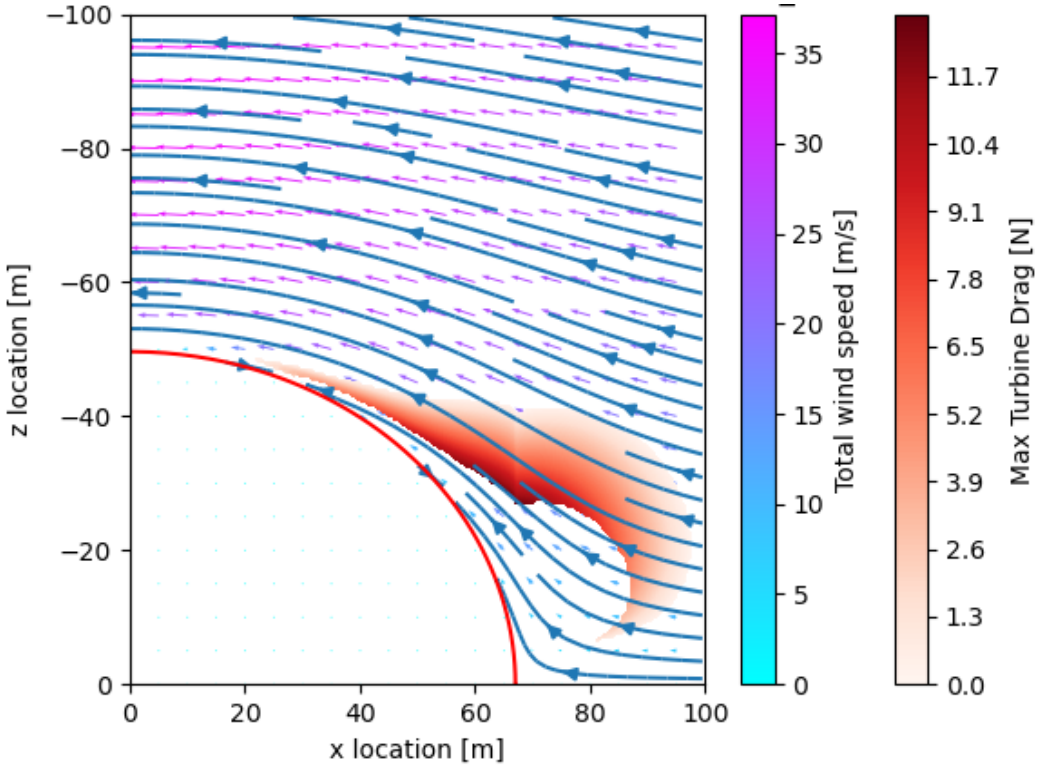

Figure 13: Plot showing complete results of the wind field program. Turbine drag is in red, streamlines in blue, wind speed and direction in shades of cyan-purple and the ship approximated as a curved red line.

With the wind field known, the second part of this program calculates the region where an aircraft of known parameters will be capable of stable unpowered flight (static soaring) and what amount of additional drag can be applied by the generator turbine to the airframe. It requires the simplified design of the aircraft to be supplied for use in the calculations. The mass and wing area of the aircraft are the main variable inputs. A description of the lift and drag of the airfoil and body are

also necessary inputs. The result of this program is a matrix of wind speeds and necessary rotor drag values corresponding to all points around the ship in 2D.

2.5 Aircraft performance calculations

Several additional considerations had to be made for the performance of the aircraft and they are covered in this section. First is the calculation of the glide speed. Then the process for determining the cruise power from the rotor performance results is described. Finally the simple model used for determining the motor/generator efficiency is explained.

2.5.1 Glide speed

The glide speed is the speed of airflow over the wings that the aircraft needs to be able to glide. This determines whether the aircraft is able to remain airborne at the ship without using the motor. When attempting to charge at the ship, if the airspeed in the stable region falls below this value, the aircraft will need to expend power to stay airborne. When using the rotor as a wind turbine, the minimum glide speed is not typical of regular flight. Therefore the minimum glide speed in those cases is determined by the wind field program as the slowest upstream wind speed that produces any soaring region at all. For the solar-only configurations, the glide speed is a simple approximation based on the need for the total lift to be greater than the weight of the aircraft and is shown in Equation 24 which is based on Equation 9. In this equation, $m_{aircraft}$ is the mass of the complete aircraft, g is gravitational acceleration and 'S' is the area of the wing.

$$U_g = \sqrt{\frac{2 \cdot g \cdot m_{aircraft}}{\rho \cdot C_l \cdot S}} \tag{24}$$

2.5.2 Cruise Power

The amount of mechanical power that must be provided by the rotor in flight is calculated based on the thrust needed to overcome drag at cruise speed. The drag is calculated using Equation 10. The value for C_d is taken from the same airfoil data source as the rotor airfoil data and is linearly interpolated such that the values represent the correct Reynolds number [14].

Once the drag on the aircraft is known, the required value of thrust to overcome it is also known because these values are equal. To find the rotor mechanical power, the desired thrust is found on the λ-thrust results of the rotor BEM calculation from Section 2.3 which gives the value for λ. Figure 14 is a plot of the λ-thrust results from a particular rotor which is used as an example to illustrate this process. With the proper value for λ it is then possible to look up the required power from the λ-power data from the same rotor design with Figure 15 being the example plot for this step. Keep in mind that the rotor calculations define regeneration mode as positive thrust and power so forward thrust will be negative and have negative power. In this example a thrust of 2N is desired to maintain cruise speed and the example plots, Figure 15 & Figure 14, show the points where this is achieved.

2.5.3 Motor/Generator efficiency

The efficiency of the motor depends on the design of the motor but also on the conditions it is operating under, so in accordance with the goals of this project, a model for various potential motors was used. This model is applied both when propelling the aircraft and when generating electricity through the rotor.

There are three main motor parameters provided by manufacturers to calculate motor performance. The kV rating describes the number of rotations per minute the motor will produce per volt applied, also shown in Equation 25. The no-load current i_o describes the amount of current required to run the motor at standard conditions with no rotor attached. This represents the mechanical losses of the

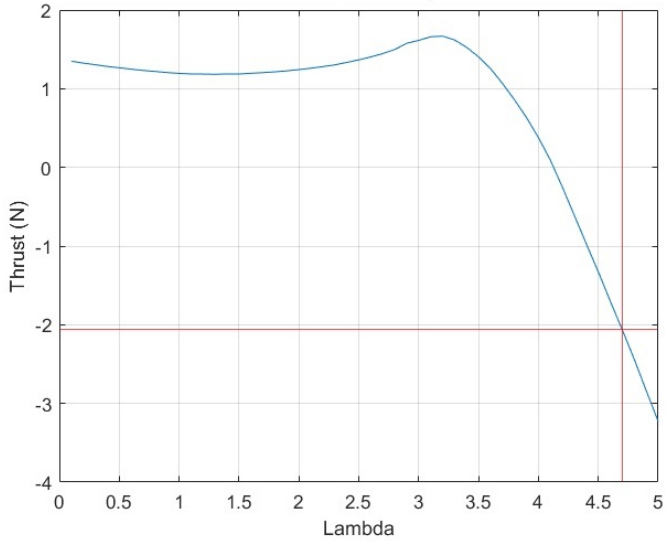

Figure 14: Intersection point for a desired thrust value of yields the value for lambda.

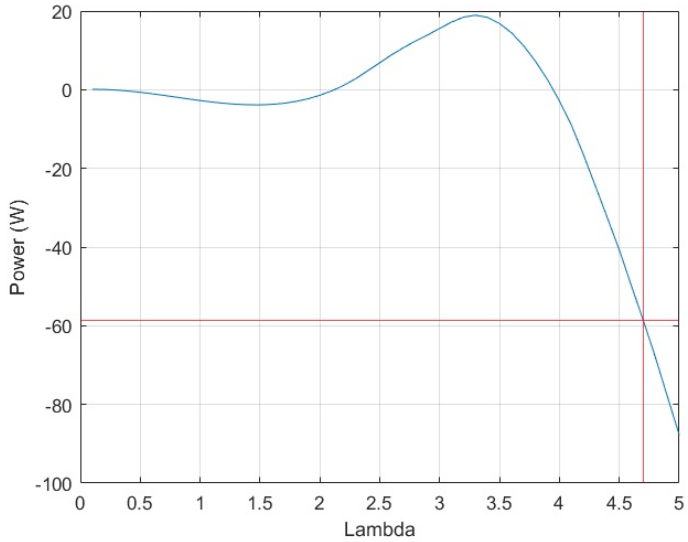

Figure 15: Intersection point for known lambda value yields the mechanical power generated by the rotor.

motor. Lastly is the winding resistance R_m which is simply the electrical resistance of the wires in the motor.

$$RPM = kV \cdot V \tag{25}$$

These three values allow the calculation of the performance of the motor in both forward flight and regenerating modes following the simple equation numbered Equation 26 [15].

$$P_{out} = P_{in} - P_{iron} - P_{copper} \tag{26}$$

where iron losses are described by Equation 27 and copper losses by Equation 28 [15]. Here, V is the voltage applied to the motor by the motor controller or the voltage generated by the motor when charging the battery. It should be noted that the definition of iron losses in this context should not be confused with the more specific definition where iron losses represent only eddy currents and magnetic

losses of the iron components of the winding armature. In this case it refers to all the losses that occur from the rotation also including friction and other physical resistances of the motor [15].

$$P_{iron} = V \cdot i_o \tag{27}$$

$$P_{copper} = \frac{V^2}{R_m} = i \cdot V = \tag{28}$$

To calculate the power used in forward flight these equations can be combined into the form of Equation 29 with V being found using Equation 25.

$$P_{out} = P_{in} - V \cdot i_o - \frac{V^2}{R} \tag{29}$$

Which can be re-arranged with some substitutions of Ohm's law into the quadratic form:

$$0 = (\frac{-R}{V^2}) \cdot P_{in}^2 + P_{in} - (P_{out} + V \cdot i_o) \tag{30}$$

Finally solving Equation 30 for P_{in} using the quadratic equation will yield the amount of electrical power required to operate the motor and propeller at the desired speed. In this case, P_{out} is the mechanical power produced by the motor and it is already known as the power required by the rotor found by the methods described in Section 2.5.2.

To calculate the amount of power that can be created by the motor when in regeneration mode Equation 29 can be used with P_{in} being the known mechanical power produced by the rotor and P_{out} being the amount of power being sent back to the batteries.

Additionally, an efficiency value of 95% is applied to the electrical power flowing through the motor controller in either direction to account for the switching losses. This approximate value is in line with available switching power supplies [16] and brushless electronic speed controllers [17]. These devices have a flatter efficiency curve than the motors which justifies the use of a constant efficiency value.

2.6 Implementation in code

Using MATLAB (or any sufficiently capable math program) it is possible to quickly calculate the performance of a given rotor configuration based on the equations of Section 2.3.1. The program used to calculate propeller performance is run for wind speeds in increments of one, up to the maximum wind speed experienced in the wind data used in the simulations. It is also important to check that the maximum wind speed here is also greater than the maximum wind speed of the output of the wind field program to prevent any gaps appearing in the performance data.

The rotor experiences vastly different Reynolds numbers throughout the range of operation. This is accounted for by using multiple sets of lift and drag data from airfoiltools.com [14] and interpolating between these sets as needed. This resource contains the shapes and accompanying aerodynamic properties of many airfoils all having been calculated by the common software tool Xfoil [14]. Aerodynamic properties of the airfoils at this source are available for Reynolds numbers between 50,000 and 1,000,000 and they are readily available to fit the range experienced by the different rotors tested.

The propeller program does not need to run at the same time as the simulations. Multiple propeller designs can be calculated beforehand and saved to be used as inputs to the simulation of the aircraft later on. This saves significant computer time. The wind field program is also run separately in advance of the full simulations. There are only a few combinations of inputs to this program so it is easiest to run it for all possible combinations and store each set of results to use in the scenario simulations as needed.

Once the program is running, the desired propeller data and wind field data is loaded into the simulation. From here these sets of data need to be sent through a matching and interpolation script. The wind field program outputs two matrices of values for a grid of points in space around the ship: drag, and wind speed. The rotor performance program calculates the drag and power profiles for a variety of wind speeds. These two sets of data must be compared to find points such that the wind speed at a point near the ship produces a propeller performance profile that has a drag value that also matches the rotor drag value from the wind field program for the same point in space.

With these points of drag congruency found, the corresponding power value, at the same operational state of the rotor, can be saved as a potential generator power value for the upstream wind speed that was used as an input to the wind field program. Depending on the inputs to these programs, the match points can number from tens to thousands. These match points are then adjusted by including the motor efficiency at these operational states. Any remaining points that have positive power are sorted. The top 2% of this list is averaged for each upstream wind speed and used as the generator power for the simulation.

The remainder of the calculations are specific to the simulation case study presented in Section 3.1.

3 Mission simulations

This chapter starts by presenting the case study and describes all the specifications applied to the model. Following that is a detailed explanation of what results are produced from the simulation through the use of a single baseline case. After that come tests of every design variable in two scenarios: one where the aircraft operates independently of the mothership, and one where they work together to maximize aircraft success. Each scenario tests the three power configurations and concludes with an optimal design. Finally an alternate approach to the energy generation for the aircraft is tested and optimized.

3.1 Case study description

As partly described in Section 1.2 this project is centered on determining the fitness of the "never landing drone" to perform a long-term mission over the sea. Further details of this case study and how the model is applied are in this subsection. First the specifics of the missions are given followed by the design of the aircraft used in the simulation. Following this is the description of the steps taken to specify the design and source of the airfoil. Finally, the design of the experiments that are performed is presented and explained.

3.1.1 Design of the mission

To gauge the success of the two generation methods, a year-long simulation attempting constant flight is used. In this simulation are two bodies: the NLD, and the mothership from which it is launched. Each craft has their own mission to perform but the aircraft always returns to the mothership to soar (saving energy) and charge its batteries in the air updrafts flowing around the ship. The cruise speed of the aircraft in all scenarios is maintained at 20 m/s as a request from the MAVLab so that it may operate in the high winds over the sea and maintain pace with the mothership.

For each of the simulations the mothership is assumed to be sailing continuously in a circle with a period of 24 hours. This circle is assumed to originate from and return to the docks at Den Helder though the process of docking and re-supplying is ignored in the simulations. The ship speed is 7.5 m/s and taken from the specifications of the Dutch Coast Guard ship Guardian [18] which the MAVLab operates on for tests. This is a simple description as there is no way of knowing exactly the route the ship would take or which ship it would be and it would ultimately be up to whoever would use such a system. The specifics of the mission are not part of the scope of this project. The direction of the mothership is important as it interacts with the ambient wind in the area. Because the relative wind that impacts the ship depends on the speed and heading of the ship in addition to the speed and heading of the wind, the ship has the option to alter its course to improve the wind conditions for the aircraft. When the ship cooperates with the aircraft the aircraft gets a boost to its soaring region and an increase in generating potential if the aircraft is recharged by its rotor. However, altering the ship's heading affects it's ability to perform it's own mission. Therefore, two scenarios are tested: one in which the aircraft and ship coordinate to improve the aircraft's performance, and a second scenario in which the more desirable case of the ship and aircraft operating independently is simulated.

The wind data used in the simulations comes from a meteorology station off the coast of the Netherlands near Den Haag [19] and consists of a full year of hourly data. The data comes from the year 2011. Solar insolation data from the island of Texel, north of the Netherlands and in the North Sea, is used as that is close to the mission location while still being on land (a requirement from the PVGIS [8]). Figure 16 shows a plot of the GHI used for the project over the course of one year.

Throughout each simulation certain metrics are recorded which constitute the primary results. The relative velocity of the wind to the mothership is recorded as this is the source of energy for the aircraft. Any time spent with a dead battery is recorded and marked as 'failure time,' this keeps track of the frequency and distribution of failures. Mission time is recorded as the main metric of success while minimizing and predicting failures is the second measure of success. Time spent charging or loitering

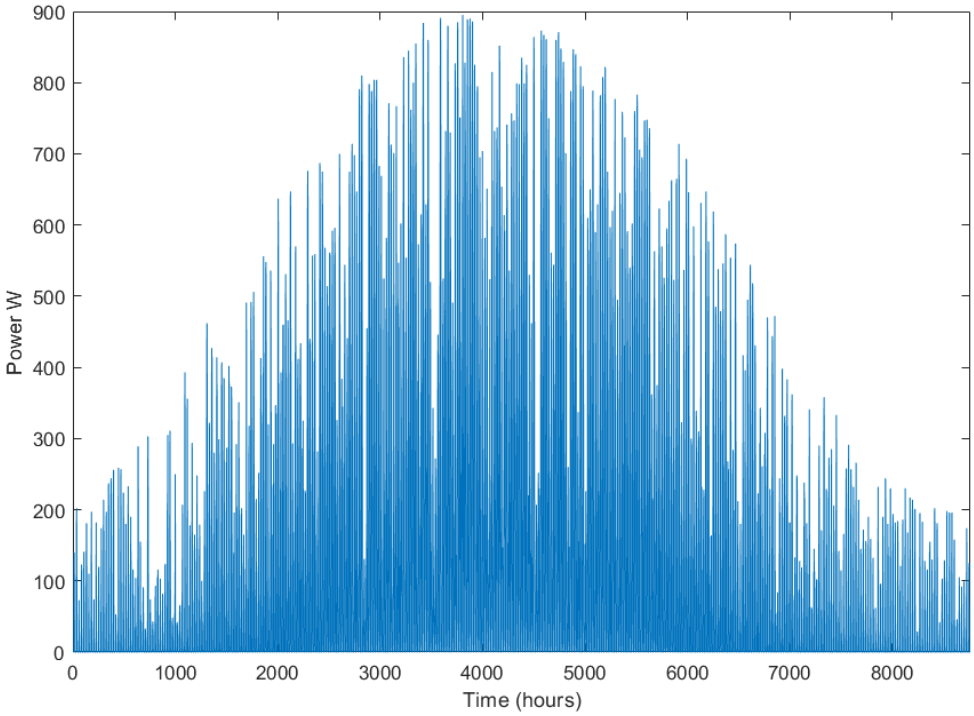

Figure 16: A plot depicting a full year of solar irradiation (GHI) from the island of Texel.

at the ship and the battery level are next. And lastly the rate at which energy is being generated and expended is recorded.

In the case where the battery is totally drained and the aircraft is unable to maintain flight then the aircraft is marked as in a failure state until conditions are good enough to relaunch and recharge in air. The aircraft is relaunched with a nearly discharged battery to prevent crashing from becoming a source of energy to improve mission time. The decision was made to launch the aircraft with a nearly depleted battery because early runs saw significant amounts of mission time resulting from fresh batteries being installed after every crash. This cannot be allowed as it defies the mission requirement that the aircraft not land at or be recovered by the mothership. Recovery and relaunch is physically unrealistic.

3.1.2 Aircraft design and control

The design of the aircraft is very simple. It follows the basic shape of a glider and is assumed to have all control surfaces necessary. It's shape consists of only a few parameters. Several parameters are part of the design variables and some others are affected by changes to the design variables. All parameters and any fixed values are listed in Table 2.

The wingspan is taken from a competition glider [20] that forms the basis of the design while the wing area varies by changing the chord. Similarly the base weight of the airframe also comes from these specifications. The wing airfoil used is the MH32 airfoil which is common in competition gliders of an appropriate size for this project [21].

The mass of the aircraft is further modified by the components added to it. Additional components can vary significantly in weight and function depending on the desired cost of a physical design and overall mass is the design variable, so the mass of additional components is not calculated with the same rigor as other metrics. The presence of solar panels on the wing is accounted for by using the area of the wing, the density of silicon and the thickness of a silicon wafer to come up with the value 0.466 kg/m^2 of additional mass. This assumes an uncovered and unlaminated panel which would be integrated into the wing. Furthermore, the mass of the battery is then whatever is left over from the

Parameter	Value
Wing span	3.2 m
Wing area	varies
Wing airfoil	MH32
Body diameter	0.1 m
Body drag coefficient	0.01
Idle power use	5 W
Mass	varies
Solar cell mass	varies
Battery mass	varies
Battery voltage	varies
Motor	varies
Cruise speed	20 m/s

Table 2: All parameters used to describe and model airframe performance are shown here.

design mass after the airframe and solar cells are removed. The battery capacity is calculated using the specific energy of 150 Wh/kg for lithium batteries which is a mid-range value of what is possible [22].

A selection of 43 motors taken from multiple manufacturers including T-Motor and Cobra motors, which are both used in the MAVLab, were chosen and their specifications were entered into the program. As explained in Section 2.5.3 these specifications will affect both the cruise power and the generator power.

The efficiency of the solar panels used is 20%. This is a common and not exceptional value for the efficiency of crystalline silicon solar cells. At least 25% conversion efficiencies have been managed with silicon solar cells [23]. Better, but more expensive, technologies exist such as multi-junction cells or the III-V family of technologies (so named because of their elemental position in the third and fifth columns of the periodic table) have a higher efficiency [23]. Thin-film panels can also be used, due to their flexibility, to cover a larger area of the aircraft without gaps. Because of the wide variety of available technologies and their differing performance, a generalized 20% solar conversion efficiency over the area of the wing is considered to be a realistic value and if desired has the capability to be made higher or lower in a more detailed design and analysis of a particular aircraft with specific solar technologies.

The control and flight of the aircraft is modeled fairly simply. Ground speed is ignored in favor of airspeed for which the exact power requirements are known as shown in Section 2.5.2. The aircraft flies a fixed amount of time (30 minutes) to some undetermined distance from the mothership and maintains this temporal distance until it is time to return to the ship to charge. While at the ship it will charge if the wind conditions allow it and otherwise will fly under its own power, waiting for more favorable winds to produce a better updraft. It is assumed that the aircraft is capable or staying within the desired region of the wind field above the ship and no consideration is given to the finer dynamics of flight as a detailed flight controller is part of the larger project which belongs to other researchers.

Included in the simulation is a simple prediction algorithm for the aircraft charging ability. The aircraft will return to the ship to charge when it has enough charge to return plus ten minutes, or if it predicts that it will be unable to statically soar at the ship until the next charging opportunity if the battery drains any further. This is useful for example, for the solar aircraft which needs to maintain a full battery (or otherwise sufficient charge) to last through the night. This calculation is based on last known wind speed at the ship and the ability to predict the solar cycle.

3.1.3 Rotor information

Choosing the correct airfoil for the rotor is difficult. Few propeller manufacturers are willing to disclose any information regarding the design of their product and none are willing to share the exact airfoil designation or description. However, APC propellers do state that their airfoil is closest to the NACA 4412 airfoil which is what is used throughout this project [12].

Lift and drag data for the airfoil used were obtained from the database at airfoil tools.com which itself obtains it from running the airfoil performance software known as Xfoil. This software is considered accurate up to the stall region [14] [24]. In order for the solver used in this project to converge to a proper solution however, performance data past the stall region is necessary.

Lift and drag coefficient polars across the full 180 degrees range of potential angles of attack are rare and not easily solved computationally [14]. Such is the case for the chosen NACA 4412 airfoil. An approximation had to be implemented for the missing range of aerodynamic data. For this reason, all lift and drag values are approximated past the stall point as a sine wave. This choice is corroborated by a report on aerodynamic measurements over a full 180 degrees [25] which showed empirical data that closely matched this approximation. The peak of the sine wave for lift is the maximum lift point and for drag it is at an angle of attack of 90 degrees. For the peak drag coefficient, the value is chosen to be 1.8 which is the same as a flat plate and also coincided with the above paper [25]. A comparison between the initial data and full approximation for drag is shown in Figure 17. Only a small portion of the design space results in using these approximated values, however their existence is necessary for the solver to converge to a solution for the overall performance. Additionally, all power generation occurs when the blades are in more favorable conditions (see Section 3.2) so the effect of this approximation on the final simulation results is minimal.

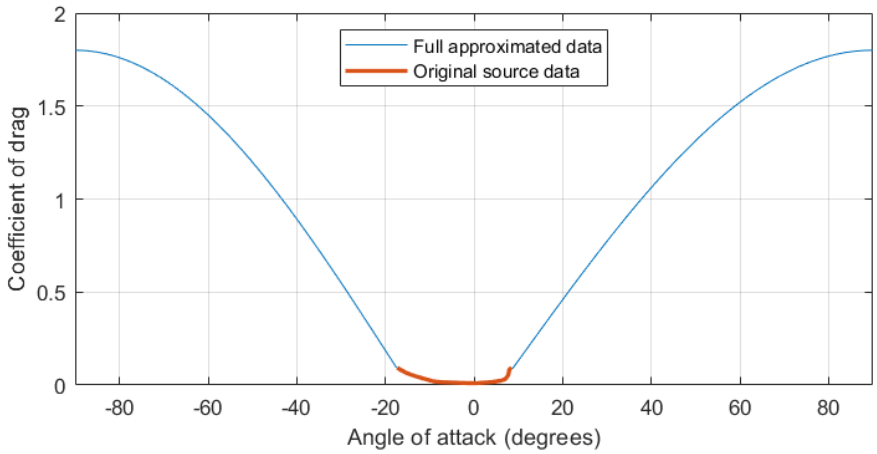

Figure 17: Plot showing original drag coefficient data from source and the complete approximation of the drag coefficient for the NACA 4412 airfoil at a Reynolds number of 200,000.

The blade chord is a generalization of measurements taken from propellers manufactured by APC. These come from a common product line which all have similar form and the airfoil used in this project. The chord shape is linearly scaled from the measurements based on the diameter. The twist is calculated based on a constant pitch as described by the propeller specifications. Pitch in this case is exactly the same as the pitch of threaded screws, that is, it is the distance traveled forward by one rotation. As such the twist angle can be calculated using Equation 31 where Θ represents the pitch in inches as given by the manufacturer. This description of blade twist is used to assist customers in picking the propellers most suited for their needs. However, this explanation (and calculations in Section 2.3.2) leads to some ambiguity whether it is a complete description. If one were to expect to make calculations of achievable flight speeds based on the specified pitch then this description would be incomplete as at any calculated pitch speed, the blade would have an angle of attack equal to zero and the rotor would produce nearly no thrust. It is because of the ambiguity on how pitch relates to

rotor geometry that additional tests have been included to consider the more likely possibility that there is additional twist in the blade. The diameter, pitch, extra twist, and lastly blade number are the variables which are adjusted in the detailed tests of the rotor. These, with the exception of extra twist, are the only variables available when choosing from pre-made APC propellers.

$$\theta = tan^{-1}\frac{(\Theta \cdot 0.0254)}{2 \cdot \pi \cdot r} \tag{31}$$

3.1.4 Design of the experiments

To determine the impact of the design variables, each is tested separately. The full set of individual tests is performed for both the cooperation scenario and the scenario where the ship and aircraft operate independently. There are many variables which could be chosen for testing but those tested in this report and their values are found in Table 3 except for the motor choice which has many more options and can be found graphically in Figure 24 or explicitly listed in Appendix A.

Variable	Diameter (in)	Pitch (in)	Extra twist (degrees)	Blade number	Wing area (m^2)	Mass (kg)	Battery voltage (V)
Minimum value	7	4	-4	2, half chord	1	3.7	11.1
Middle value	10	7	0	2	1.25	4.7	14.8
Maximum value	14	10	4	3	1.5	5.7	22.2

Table 3: Displayed are all design variables (except motor choice) and the potential values used for testing.

These design variables were chosen because they are likely to affect performance, are the given specifications of available components, or are otherwise of interest. Diameter, pitch, motor, and battery voltage are the variables which are based on discrete industry standard available components. Wing area, and mass are design choices that can be any value but are limited by the desired mission. For example, a mission where the mothership had a landing pad would change the potential designs. The MAVLab has placed constraints on some aspects of the aircraft design such as the wingspan and overall size so that it can fit on and be launched from any naval vessel. Lastly, blade extra twist, number of blades and chord length are parameters with uncertain origins or impact and were chosen for further investigation.

Propeller diameter and pitch can be found in almost any value but a range of 7-14 inches and 4-10 inches respectively account for most "normal" designs of this size aircraft. Additionally, most propellers have 2 blades but designs with three or four blades also exist with decreasing commonality as more blades are added. To account for the lack of single bladed propellers, a thin 2-bladed propeller is also modeled to have three data points for a trend.

As the design of the aircraft is based on an existing competition glider the range of values for the aircraft parameters are based on that design. The reference aircraft had a weight of 2-4kg so the weight of the modeled aircraft is increased to try values between 3.7 and 5.7 kg to account for a much larger battery and the additional solar hardware. The wing area was increased from $\frac{2}{3}m^2$ to a minimum of 1 m^2 and a max of 1.5 m^2 to account for the higher mass, necessarily low glide speed, and to give the opportunity to have more solar cells. Lastly, lithium batteries are the current standard in smaller drones and exist most commonly in the three pack voltages used here corresponding to 3, 4, & 6 cells in series.

All variables are adjusted in turn for each of the three power generation configurations which are wind turbine only (hybrid rotor), solar panels only, and both power systems combined. Values outside of the ranges listed in the table exist and may or may not improve performance further. Because of the large selection of motors, each set combination of the other design variables is run through the simulation for every motor and only the results from the best motor are chosen. The definition of 'best motor' is whichever one produces the highest mission time though the best motor also always has the lowest

failure percentage as well. The purpose of these tests is to determine how each design variable affects performance to discover avenues of improvement.

3.2 Baseline case and detailed performance explanation

The baseline case here will be explained in-depth to introduce the format of the results of the model. This scenario is using both wind and solar generation, and the aircraft and ship cooperate to serve as an example of most of the potential dynamics of the simulations. The design inputs can be found in Table 4 and are the default values used in all simulations when not being individually varied. The main results of the baseline case which will be shown for all other cases can also be found in the table.

Variable	Value
Diameter (in)	10
Pitch (in)	7
Extra twist (degrees)	0
Blade number	2 Blades
Wing area (m^2)	1.5
Mass (kg)	5.7
Battery Voltage (V)	22.2
Mission time	35.7 %
Charging time	64.3 %
Failure time	.008 %
Mean charging rate	38.2 W
Cruise power	71.4 W
Best motor	#31

Table 4: Inputs of baseline case simulation and the corresponding main results.

Based on the above parameters the rotor performance and near-ship wind field values can be calculated before running the simulation. Running the matching algorithm as described in Section 2.6 results in a set of matches for each upstream wind speed which can be plotted as has been done in Figure 18. Because each upstream wind speed results in a range of local wind speeds near the ship there is a range in potential power profiles that the rotor can operate in, the maximum and minimum of which are shown as the two lines in the graph. All match points are shown between these profiles and the distribution across the x-axis shows that the rotor is typically able to operate near it's maximum power. In this case, the maximum power for both wind speeds is near a lambda value that is roughly the center of the match points. This is generally true for all of the rotors and conditions tested.

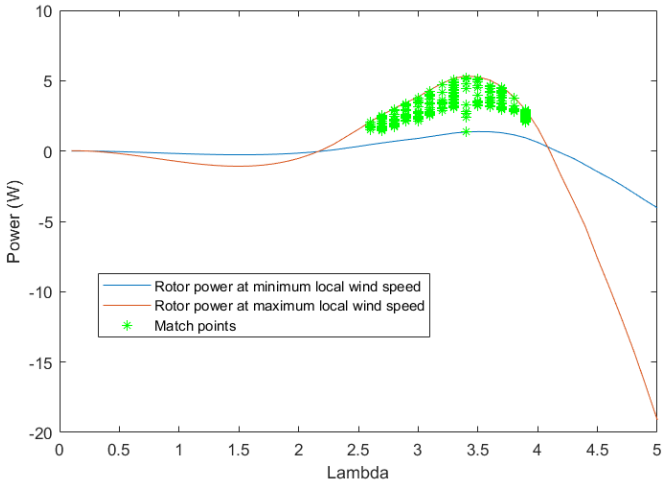

Figure 18: Plot showing potential turbine power operating points with limiting regions shown for 10 m/s upstream relative wind velocity.

More points will generally be found for rotors that can generate more electricity because higher peak power correlates to a greater difference in maximum and minimum rotor drag for each wind speed. This effect can easily be seen in Figure 23 where a plot of the drag for the same rotor across two wind speeds is shown. In that figure, the maximum drag increases far more than the minimum drag resulting in a larger drag range. A greater range of potential drag values means more opportunities to find a match with the required drag of the soaring region.

The points across all cases have a similar distribution but in some situations the blue line is flatter making it seem like the points have shifted up when in reality, the points are roughly the same but the envelope has widened. Again, this is because higher wind speeds result in a greater range of drag, and lower wind speeds result in a smaller range where the minimum drag is quite close to the maximum. In these cases, there are no matches because the rotor minimum drag is greater than the maximum allowed soaring drag. Some additional information on this subject can be found in Section 4.1 where the result of a design outside the chosen values is explored.

Taking the average of just the top 2% of match points produces a relationship between upstream wind speed and available power. This relationship is plotted in Figure 19 and used throughout each case's simulation and is unique to the design of each case including the motor choice as they affect the ability to find a match between the necessary drag and the capabilities of the rotor while still generating electricity. It can be the case where there is a stable soaring region and the rotor can match the needed drag but the low rotational speed and power would result in the motor being unable to convert the available mechanical power to electricity. The match region in Figure 18 shows points with higher power than Figure 19 because the final power graph includes the efficiency of the motor. At low wind speed and angular velocity shown in these figures, roughly half of the power is lost.

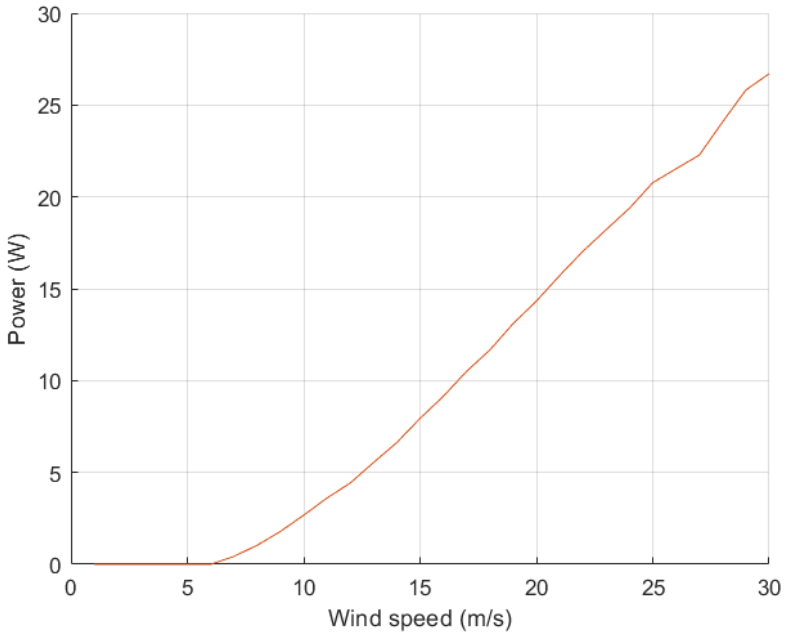

Figure 19: Plot relating upstream relative wind speed to available wind power for the set of design inputs in Table 4.

To display the details of what happened through the simulation two grouped plots are shown. Figure 20 shows the state and performance of the aircraft over the full year of the simulation for an idea of the seasonal trends and behaviors and Figure 21 shows a selection of a few days where more detail is visible. To interpret these plots some explanation is required. The top-left graph shows the relative wind speed between the ship velocity and the natural wind velocity and also what the relative wind speed is when the ship turns to face into the wind constituting the process of cooperation with the ship. For the "Mission", "Charging", and "Failure" plots, in Figure 20 attention should be paid to the distribution of states. Each of these register a 1 when the aircraft is in that state at that time and zero otherwise. When observing these state plots, not enough detail is present when viewing the entire year to see any length of time spent at each state. Instead, the states appear as vertical lines allowing a feel for the frequency of the state rather than its length. The clearly more dense areas near the center of the time period in Figure 20 show that the aircraft is most active during the summer. The explanation for this activity comes from the bottom-right graph which shows the amount of energy that the aircraft is able to gather throughout the simulation which is also heavily influenced by summer sunlight. Lastly, the bottom-left plot shows the state of charge (SOC) of the battery which in this case is not very informative. It is more useful to view this and the three state plots over a shorter period of time.

Focusing on Figure 21 now, much more detail about what is happening throughout a day can be seen. The relative velocity shows that the ship will only change direction to improve wind speed when the aircraft is attempting to charge but the natural wind speed is too low. What can be seen in the battery status plot is the flat regions of maximum charge where the sunlight fully charges the battery and exceeds the aircraft's energy demands for a time. Once the sun goes down, the battery drains relatively quickly until the aircraft returns from the mission state (top-right) to the charging state (middle-right) where its energy consumption drops significantly and some charging from the hybrid rotor may occur. In one instance, the battery discharges fully and the result is a mission failure (shown in middle left plot) but the failure only lasts a very short time as conditions soon improve enough to return to flight. Some potential improvements to the model and simulation are revealed by these detailed plots which will be discussed in Section 4.2.

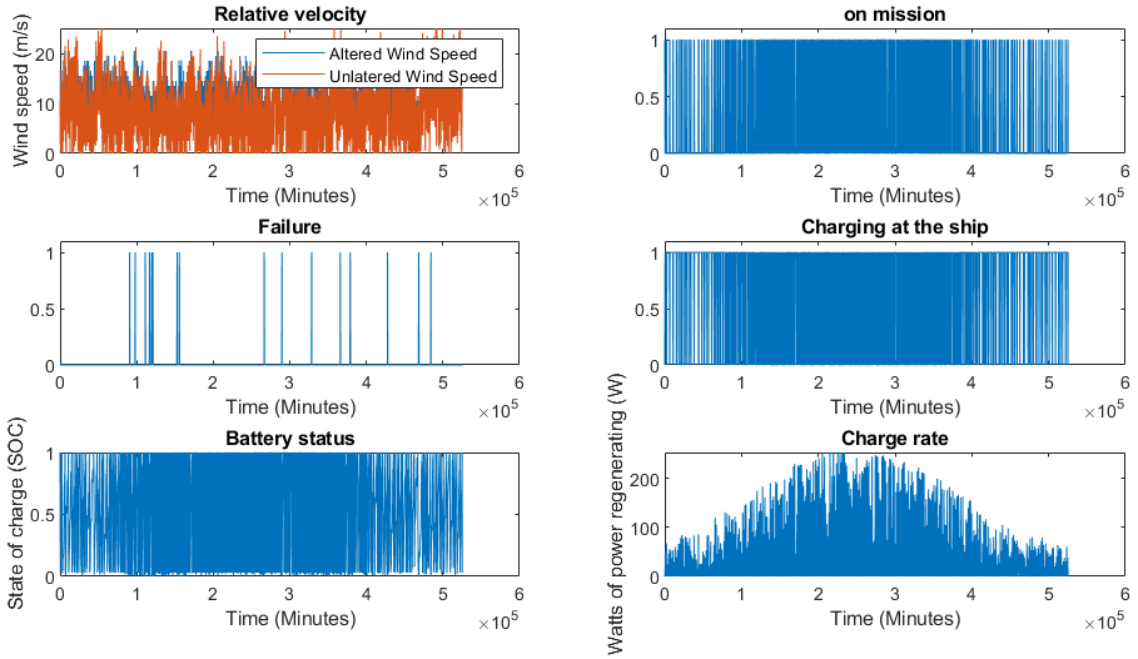

Figure 20: Detailed plot showing the status of the aircraft throughout the full year simulated. At this level of magnification, seasonal trends become apparent as the density of lines except for the bottom right plot which directly shows the generated power.

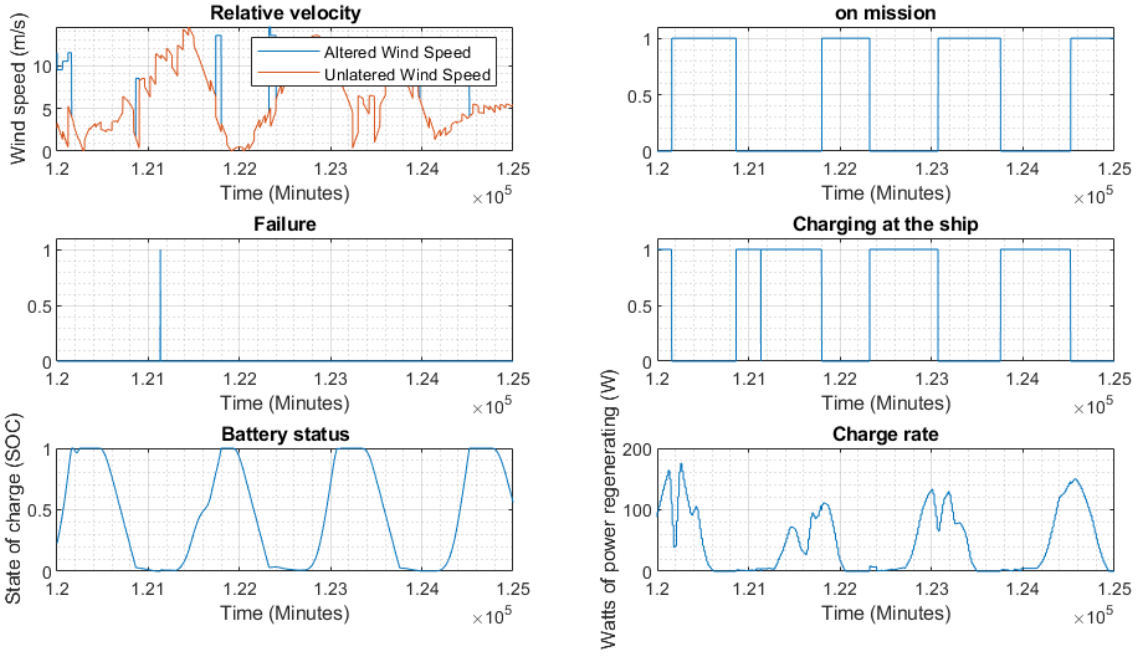

Figure 21: Detailed plot showing the status of the aircraft over a period of 4 days. At this level of magnification, hourly trends and exact operational states can easily be seen.

3.3 Independent ship and aircraft scenario

The first scenario is a situation in which the drone is intended to operate independently of the mothership and vice versa. Each design variable is varied in turn. After that, the trends shown are used to produce some optimized designs for the three generation methods.

3.3.1 Detailed tests

The full simulation is run for each generation method testing each design variable in turn to produce the results shown in Table 5. The percent of time the aircraft spent on mission and percent spent with a drained battery (marked "Failure") are recorded for each generation method. Additionally, the mean charge rate and best motor, are recorded for each generation method. The cruise power is in the final column because it is not dependent on the generation method so it only needs to be shown once.

What should be immediately obvious is that the mission percentages for the hybrid rotor configuration only exceeds 1% once and the failure rates are consistently very high. These two columns are some of the most critical results of the whole report as they represent the tests that are closest to the ideal version of this project but final conclusions can only be drawn after the optimized tests below. The solar and combined configurations both perform much better than the hybrid rotor configuration but neither are able to reduce failure rate much below 20%. The effect of the combined power systems on the mean power generated is mostly just the addition of the separate wind and solar powers. However this is not the case for the mission percentages. The best cases result in a maximum mission time of 1.8%, 19.2%, and 25.7% for wind, solar, and the combined system respectively. This shows that there certainly is a synergistic effect within the simulation as the combined system does better in this metric than both separate systems' results added together.

With the design of the rotor, increasing the diameter increases the power needed for forward flight but also increases the wind collection area when regenerating. As shown in the table, the hybrid rotor aircraft sees an overall benefit from a larger rotor while the solar aircraft sees a benefit from the reduced cruise power of the medium-sized rotor. Going too small requires an increase in power again. Both cases show only a small difference between the two smaller designs and a more significant difference with the larger rotor. Because the effects of rotor diameter on generation and on cruise power do not follow the same relationship, the opposing needs of the differing generation methods do not cancel out. This results in the combined generation aircraft still favoring the larger rotor diameter but not by very much. The failure percentage is particularly sensitive to rotor diameter as a larger rotor can help keep the aircraft supplied with enough power to soar during the night until the sun rises.

Variations to the pitch of the rotor have the opposite effect on mission time in the hybrid rotor and solar crafts because the increased wind power generated by the small pitch rotor benefits the former while increase to the cruise power harms the latter. This leads to the combined system favoring the medium or higher pitch rotors. The combined system experienced very little change to the generation rate from the wind generation component despite the changes in pitch.

		Hybrid rotor wind generation				Solar generation				Wind and solar				Cruise power
Variable	Value	Mission (%)	Failure (%)	Motor (#)	Mean charge rate (W)	Mission (%)	Failure (%)	Motor (#)	Mean charge rate (W)	Mission (%)	Failure (%)	Motor (#)	Mean charge rate (W)	(W)
Diameter (in)	14	1.81	24.2	24	8.2	13.9	40.1	31	30.9	25.3	16.6	24	38.1	92.3
	10	0.11	38.1	37	3.5	18.0	35.6	31	31.8	24.8	21.4	5	34.6	73.6
	7	0.06	65.4	5	0.5	17.6	36.1	5	31.7	19.0	36.9	29	31.4	72.9
Pitch (in)	10	0.06	44.2	31	2.3	19.2	34.6	31	32.0	25.2	20.9	5	34.1	67.5
	7	0.11	38.1	37	3.5	18.0	35.6	31	31.8	24.8	21.4	5	34.6	73.6
	4	0.19	37.9	29	4.1	13.1	40.7	24	30.7	19.3	26.2	29	34.2	99.9
Extra twist (degrees)	+4	0.28	32.1	37	4.5	15.8	38.2	5	31.4	24.0	19.8	37	35.3	82.3
	0	0.11	38.1	37	3.5	18.0	35.6	31	31.8	24.8	21.4	5	34.6	73.6
	-4	0.06	44.2	31	2.2	18.9	34.7	31	32.0	25.2	20.9	5	34.1	68.0
Blade number	2	0.11	38.1	37	3.5	18.0	35.6	31	31.8	24.8	21.4	5	34.6	73.6
	3	0.49	31.5	5	5.1	16.7	37.1	31	31.6	25.6	18.8	5	35.9	77.5
	2, half chord	0.05	49.5	5	1.6	16.4	37.4	5	31.5	21.1	26.7	37	33.1	78.1
Wing area (m^2)	1.5	0.11	38.1	37	3.5	18.0	35.6	31	31.8	24.8	21.4	5	34.6	73.6
	1.25	0.23	37.8	24	3.5	17.2	37.1	31	26.3	25.6	16.7	37	29.7	60.9
	1.0	0.47	31.3	37	4.3	15.0	39.8	5	20.7	25.7	15.1	37	24.7	51.2
Mass (kg	5.7	0.11	38.1	37	3.5	18.0	35.6	31	31.8	24.8	21.4	5	34.6	73.6
	4.7	0.08	33.3	37	3.1	17.5	36.9	31	32.0	25.1	21.9	37	34.5	75.8
	3.7	0.08	33.8	37	2.6	4.3	39.8	31	32.0	23.9	24.3	37	34.1	78.7
Battery Voltage (V)	22.2	0.11	38.1	37	3.5	18.0	35.6	31	31.8	24.8	21.4	5	34.6	73.6
	14.8	0.06	43.3	24	3.1	17.9	35.7	24	31.8	24.0	24.7	24	34.3	71.7
	11.1	0.06	43.3	24	3.1	17.9	35.7	24	31.8	24.0	24.7	24	34.3	71.7

Table 5: Results of first simulation cases of the independent ship and aircraft. Cruise power is shown in a separate column because it is the same across each of the three generation methods.

Changes to the "extra twist" component had an effect on wind power similar to the pitch as they are changing the same geometry in a similar way. It did however have a larger effect on the wind generation ability with a smaller effect on the cruise power. This indicates that it was the right choice to add it as a design variable as it is able to improve performance better than pitch can for the hybrid rotor aircraft. For the combined system the effect of extra twist follows the solar only system but with diminished effect as the hybrid rotor and solar configurations have opposite reactions to this variable.

The blade number variable had a somewhat unexpected result. In this case, cruise power was lowest for the default value which was based on the original design, though generating potential for the hybrid rotor system did increase as expected. Naturally the solar aircraft performed best with the default value, but because the hybrid rotor aircraft performed best with more blades, the combined system still favors having three rotor blades.

Moving on to the design variables of the airframe the total wing area is first. As expected, a larger wing has a lower glide speed allowing all configurations to statically soar at the ship even in worse conditions. However, the increased drag from the larger wing also had a significant impact on cruise power meaning that when soaring was still impossible, the battery was drained even faster. This meant that the hybrid rotor aircraft has significantly fewer failures with a small wing. Additionally, a smaller wing also changes the dynamics of the stable soaring region in the wind field. Less wing area means less lift and "wasted" drag meaning that the aircraft can find a position where it can apply more drag through the turbine and thus produce more energy. The solar aircraft experiences the same effects on soaring but its generating potential is directly proportional to the area of the wing so it still receives benefits from a larger wing though the difference is small. The difference in mission performance across different wing areas shrinks even further for the combined system but the failure percentage shows clearly that a small wing is better.

Next is the mass of the aircraft which also affects the size of the battery. This variable has very strange behavior. Decreasing the mass of the aircraft actually *increased* the cruise power. Investigating this behavior showed that the cause was the wing airfoil having too much lift at zero angle of attack. To maintain level flight, this required the aircraft to have a slight negative angle of attack which also forced it to have greater drag. This increased drag increased the power needed to fly. The mass of the hybrid rotor aircraft had a similar effect as the wing size such that an increase in mass also allowed the aircraft rotor to apply more drag and generate more power. This led to a slightly higher mission time but a significant increase of failure time. The solar aircraft favors a larger battery with the combined system doing best with the middle size.

Finally, the effects of battery voltage in all configurations are practically non-existent. However, any differences present do favor a higher voltage.

3.3.2 Optimized test

The trends and relationships discovered in the previous subsection can be used to inform decisions when producing some configurations which optimize for a high mission time or low failure time. This section shows the attempt to produce one of both for each generation method to see what level of performance is possible with the concepts explored in this project. The optimal designs and results are summarized in Table 6. These designs start by following trends from the individual tests above, but if those fail to produce good results or when conflicting trends obfuscate the issue, educated guesses are used to find an optimum.

The first thing to note is that for the solar and combined configuration (which is dominated by solar generation) there was no minimum failure design because no combination of design variables resulted in a lower failure percentage than the design intended to maximize mission time. This is not unexpected as traits which maximize success should overlap with those that minimize failure.

Creating an optimized design succeeded in producing results greater than any of the individual tests above but, with the exception of the hybrid rotor aircraft, these improvements are not as great as expected. The hybrid rotor aircraft gained over twice the mission time but attempting to reduce

failure rate resulted in only a small change compared to the best of the individual tests. Even with the improvement, the low mission time and high failure time of the hybrid rotor configuration is too low to be considered a successful idea. Only the combined system is considered to be close to viable.

	Mission optimized designs			Failure optimized designs		
	Wind	Solar	Combined	Wind	Solar	Combined
Diameter (m)	.3556	.1778	.3556	.3556	-	-
Pitch (in)	7	10	10	7	-	-
Ex. Twist (degrees)	+4	-4	-4	+4	-	-
Eff. Blade	3	2	3	2	-	-
Wing Area (m^2)	1	1.5	1	1	-	-
Mass (kg)	4.7	5.7	5.7	5.7	-	-
Motor	31	31	31	31	-	-
Mission (%)	5	20	29.17	4.1	-	-
Failure (%)	25.3	33.4	12.3	23	-	-
Cruise (W)	135.8	63.9	56.3	102.6	-	-
Gen. (W)	13.4	32.2	27.5	12.1	-	-

Table 6: Independent scenario optimized designs and results. Minimum-failure optimized designs were the same as the mission optimized designs for the solar and combined configurations so they are not duplicated.

Examining the details of the designs shows that the optimum hybrid rotor design is not immediately clear from the above individual tests. The need to fly efficiently and also generate electricity with the same rotor is a difficult challenge. Attempting to use multiple changes to improve the generating capability resulted in compounding significant increases to the cruise power. For example, a low value for pitch increased mission time in the individual tests but a middle value of pitch works better in the optimum design because the compounding increase in cruise power from all the variables was too great. With rotor diameter being the greatest predictor of generating potential, it is no surprise that the hybrid rotor and combined power configurations preferred a larger diameter.

The solar aircraft did follow the predictions perfectly because it had almost no conflicting needs. All four rotor design variables favored efficiency in forward flight without any compounding effects causing issues. The only exception is the wing area. A large area increases gliding capability in low wind and increases solar power generation at the cost of greater drag in powered flight. Tests showed that the effect of wing area on performance is very small because the increase in drag has nearly the same proportional effect as the increase on solar energy but the increased gliding capability still benefits the aircraft. This was not true in the individual tests because it really depends on the rotor design whether the change in drag will match the change in solar power.

Another interesting result is that the solar optimum design had a much higher failure rate than the hybrid rotor aircraft. The cause of this can be clearly seen in Figure 22. The top right graph shows that all the mission time is centered around the summer period (middle of the year) when the available solar energy is significant. During winter the battery does not even reach a full charge for a period of several months. Without effective charging, failure becomes a common occurrence.

The combined system was most interesting as it incorporated elements of both the other two configurations. A large, 3-bladed rotor which is also designed to have a pitch and extra twist more suitable for cruise flight and a smaller wing actually results in the lowest cruise power of the group. This optimum design is not significantly better when comparing mission time to the individual tests but the failure rate is significantly reduced doe to the inclusion of more wind energy generation that can sustain the aircraft through winter.

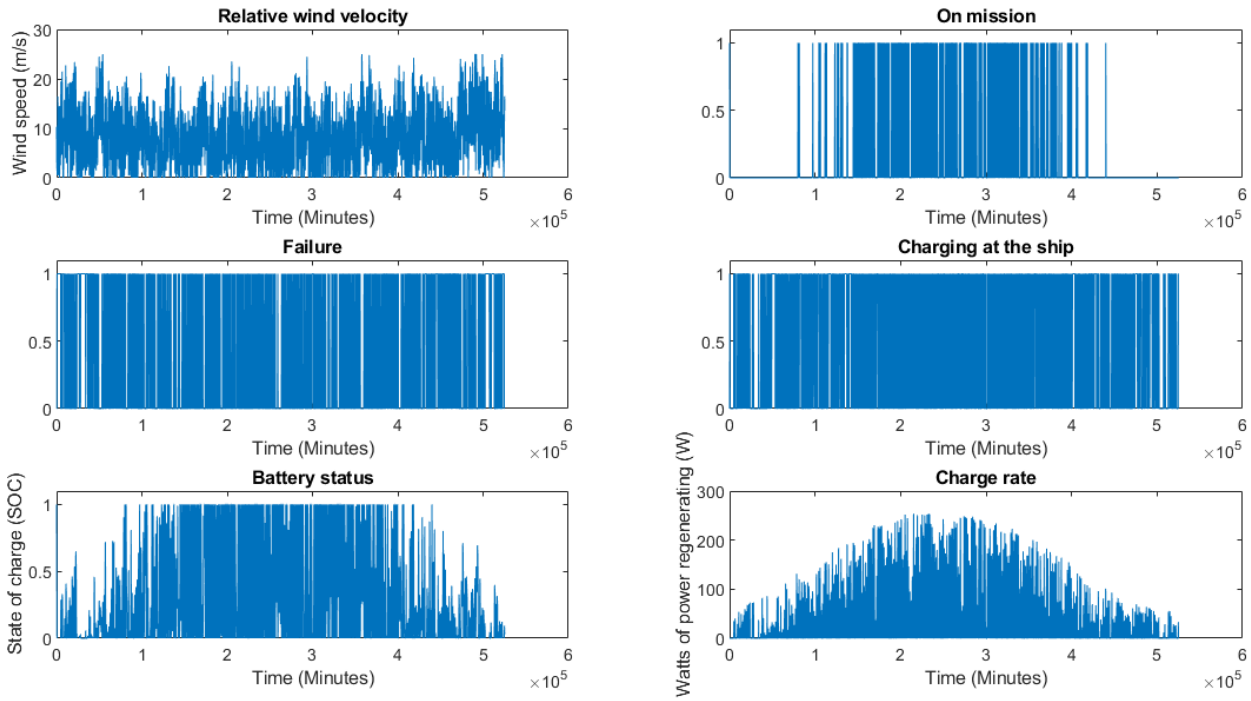

Figure 22: Plot of solar optimum design status over time. Key plots are the mission time on top right, battery SOC on bottom left and charge rate on the bottom right.

3.4 Cooperating ship and aircraft scenario

The second simulation is a situation in which the drone and ship work together to ensure that the drone does not run out of power. The ship will follow its designated path except when the drone is attempting to charge and the relative wind speed is not enough to allow the drone to hover in the updraft. In such cases, the ship will steer directly into the wind to maximize relative wind speed. As long as the percent of time spent where the ship has to alter its course is less than 50%, which turned out to always be the case in this scenario, then one can be fairly sure that the simulated ship would not be forced to run aground by continuing in an undesired direction indefinitely. This was a minor consideration as the wind conditions in the North Sea do tend towards unidirectional wind [19].

3.4.1 Detailed tests

Similar to the previous section, each case is now run in the new scenario where the ship and aircraft coordinate to improve the aircraft's survivability. The ship changes its course to improve the wind conditions for the aircraft but only when the aircraft is unable to soar at the ship in the existing conditions. This prevents the aircraft from having to fly under its own power and also improves its generating potential for the hybrid rotor cases which improves mission time.

		Hybrid rotor wind generation				Solar generation				Wind and solar				Cruise power
Variable	Value	Mission (%)	Failure (%)	Motor (#)	Mean charge rate (W)	Mission (%)	Failure (%)	Motor (#)	Mean charge rate (W)	Mission (%)	Failure (%)	Motor (#)	Mean charge rate (W)	(W)
Diameter (in)	14	9.7	0.01	31	13.3	24.9	0.26	31	34.1	35.7	0	31	43.7	91.0
	10	2.1	0.02	37	6.4	29.1	0.38	31	34.1	35.7	0.01	31	38.2	73.6
	7	0.1	11.51	5	1.5	28.7	0.36	5	34.1	30.2	2.05	29	35.4	72.9
Pitch (in)	10	0.2	0.15	31	4.7	30.2	0.44	31	34.1	35.8	0.02	31	37.2	67.5
	7	2.1	0.02	37	6.4	29.1	0.38	31	34.1	35.7	0.01	31	38.2	73.6
	4	2.8	0.02	24	7.4	24.3	0.23	24	34.1	30.5	0.01	24	39.5	95.1
Extra twist (degrees)	+4	3.5	0.01	5	7.6	26.8	0.25	5	34.1	34.0	0.01	5	39.4	81.0
	0	2.1	0.02	37	6.4	29.1	0.38	31	34.1	35.7	0.01	31	38.2	73.6
	-4	0.3	0.11	37	4.8	30.1	0.44	31	34.1	35.5	0.02	31	37.2	71.7
Blade number	2	2.1	0.02	37	6.4	29.1	0.38	31	34.1	35.7	0.01	31	38.2	73.6
	3	5.2	0.01	31	8.7	27.7	0.31	31	34.1	36.1	0	31	40.0	76.9
	2, half chord	0.1	0.59	5	3.5	27.5	0.28	5	34.1	31.7	0.06	5	36.6	78.1
Wing area (m^2)	1.5	2.1	0.02	37	6.4	29.1	0.38	31	34.1	35.7	0.01	31	38.2	73.6
	1.25	3.3	0.02	31	6.8	29.0	0.98	31	28.4	37.3	0.01	31	33.0	60.7
	1.0	5.5	0.02	31	7.5	28.3	3.19	5	22.7	39.0	0.01	31	27.7	50.9
Mass (kg	5.7	2.1	0.02	37	6.4	29.1	0.38	31	34.1	35.7	0.01	31	38.2	73.6
	4.7	1.1	0.06	24	5.5	26.7	0.44	31	34.1	32.6	0.02	31	37.9	73.7
	3.7	0.3	0.18	24	4.6	25.2	0.92	31	34.1	29.9	0.04	31	37.4	76.4
Battery Voltage (V)	22.2	2.1	0.02	37	6.4	29.1	0.38	31	34.1	35.7	0.01	31	38.2	73.6
	14.8	2.0	0.02	24	6.2	29.0	0.37	24	34.1	35.7	0.01	24	38.3	71.7
	11.1	2.0	0.02	24	6.2	29.0	0.37	24	34.1	35.7	0.01	24	38.3	71.7

Table 7: Results of the cooperating ship and aircraft scenario. Cruise power is shown in a separate column because it is the same across each generation method.

First observations show that this scenario has significant improvement over even the first scenario optimized designs. Improvements in the mission time of 50% to 500% over the first scenario tests can be observed. The failure rate has mostly been eliminated by cooperating with the mothership to support the aircraft. The only instances of significant failure rates occur when the hybrid rotor produces less average power than the aircraft uses while soaring, or due to a simulation artifact for solar planes with low cruise power values.

Similar to the first scenario above, increasing the diameter increases both the cruise power and the generating potential but the effect on generation is far greater as the ship now supports the aircraft to help it charge. The mission time for the smallest rotor did not change meaning that the rotor must have a certain level of generating capacity before it can benefit from the ship's assistance. As shown in the table, the hybrid rotor and solar aircraft see similar levels of influence from rotor diameter but in opposite directions leading to the combined system favoring the middle rotor diameter with the large diameter being close behind. Unlike the independent ship scenario, the solar aircraft sees little effect on failure time from the rotor size which also tempers the effect on the combined system.

Variations to the pitch of the rotor have the opposite effect on mission time in the hybrid rotor and solar aircraft, but the same effect on failure time. This leads to the combined system favoring the medium or higher pitch rotors. The effect on solar failure rate is probably an artifact from how its control algorithm is designed. The solar aircraft returns to the ship when it has a certain number of *minutes* of flight rather than Wh remaining. This means that once it can enter low-power soaring at the ship, an increase in cruise power from the low pitch rotor results in the same "minutes of flight" remaining but greater energy reserve. The combined system still performed best with the larger pitch and had lower failure rates with a lower pitch.

Changes to the "extra twist" had the same effects as the independent ship scenario for the wind and solar configurations but the combined system added up slightly differently resulting in the zero-added-pitch design being the best.

The blade number had the exact same effect on this scenario as in the scenario of the previous subsection.

The effect of wing area on the mission time of the solar aircraft is smaller in this scenario but still favors a larger wing. The hybrid rotor aircraft also shows the same relationship favoring a smaller wing but the result is magnified by the assistance of the ship resulting in the combined configuration showing a larger preference towards the smaller wing size to maximize mission time. Failure time did not vary significantly either way for the combined system or the wind system however the solar aircraft is significantly impacted by the lower generating potential and higher glide speed increasing its failure rate.

For the mass of the aircraft, all three generation configurations performed best with a heavier craft for both mission time and failure rate. In this case, even the improved hybrid rotor speeds from the cooperating ship are not always enough to maintain soaring for the solar craft.

Finally, the effects of battery voltage in all configurations is still very small.

3.4.2 Optimized test

Similarly to the previous section, the results and trends from the detailed tests of the cooperating ship and aircraft scenario allowed the creation of several optimal designs shown in Table 8. Again, a set of designs was made to maximize mission time and a set to minimize the failure rate. In some cases the conflicting design requirements of the solar aircraft and hybrid rotor aircraft, made trends hard to predict so several iterations were run to produce these optimized results. In this scenario, the wind generation method is far more significant than the previous simulation so the effects were no longer able to be ignored in favor of optimizing power expenditure. Iterations with finer granularity or simply calculating all combinations would no doubt produce some better designs but these results are still representative of the level of improvement that should be possible. Battery voltage was left out of

these tests as in all cases, the 6-cell battery was better but with such a small difference it was not worth testing further.

One thing that may stick out is that the minimum failure design for the combined configuration is significantly different from the other two. Initially, following the trends did result in a very high cruise power and moderate mission time of 12% but by chance, attempting to make a better mission-optimized design resulted in a 0% fail rate so that result was entered into the table. This was not unexpected because most of the combined generation results had exceedingly low failure rates already.

The combined generation mission-optimized test was a problem. No configuration was capable of beating one of the detailed tests above but the difference is only 0.043% decrease from the detailed tests above so the 'optimal' test is included here to show the alternate design. Similarly, the solar results did not have much variation so the optimized test was also very close to some of the above configurations though in this case some improvement was still possible. With the benefit of the ship, only the hybrid rotor aircraft was capable of showing significant improvement by changing the design variables. Failure rate for this configuration was already low but the optimized design was able to increase the mission time from 9.7% to 16.9%.

	Mission optimized designs			Failure optimized designs		
Inputs:	Wind	Solar	Combined	Wind	Solar	Combined
Diameter (m)	.3556	.1778	.254	.3556	.3556	.254
Pitch (in)	9	10	7	4	4	7
Ex. Twist (degrees)	0	-4	0	+4	+4	+4
Eff. Blade	3	2	3	3	3	3
Wing Area (m^2)	1	1.5	1	1	1.5	1
Mass (kg)	5.7	5.7	5.7	5.7	5.7	5.7
Results:						
Motor	31	31	31	24	24	5
Mission (%)	16.9	30.9	39	5	5.5	34.4
Failure (%)	.013	.473	.001	0	0	0
Cruise (W)	71	65.1	56.9	363.5	391	71.5
Gen. (W)	14.9	34.2	29.6	22.5	34.2	30.7

Table 8: Cooperating ship and aircraft scenario optimized designs and results.

3.5 Separate turbine capabilities

The previous sections compared the wind generation concept to the solar generation concept but did not fully explore what is gained or lost by using the same rotor for propulsion and as a wind turbine. For this section, a separate turbine rotor and generator is tested with the rotor and motor combination best suited for thrust being used to propel the aircraft. Only the wind turbine generator and combined power configurations are included in this section as a separate generator unit is incompatible with the solar only configuration.

The way that the separate turbine is modeled is quite simple; it's tested using nearly the same model and design variables as before. The key difference in the results comes from the fact that the separate turbine can now be designed with its airfoil in the correct orientation allowing for far more efficient and effective power generation. The cruise power is calculated using the lowest-power rotor design and the accompanying motor from the earlier tests. This can easily be seen in the fourth row of Table 7 from the scenario above. This propeller is used for both wind and combined configurations in this section. Both the turbine and propeller are assumed to have folding blades to eliminate the issue of the extra drag from whichever rotor is not being used at the time.

With the conflicting demands on the rotor performance removed, testing each variable becomes unnecessary. For the four rotor design variables, each are picked to have the greatest generating potential

without any negative effects. So, for all cases the turbine had a diameter of 0.3556 m, pitch of 4 in, 3 blades, and 4 degrees of extra twist added. The blade airfoil is oriented such that the upper surface faces downwind but otherwise is the same airfoil as in all other tests.

For the aircraft design variables, there is only one real consideration. The wing area of the solar aircraft has a significant positive effect on solar power generation but also negatively affects the power needed for cruising. For the combined configuration both high and low wing areas are tested. The wind power only design obviously works best with the smaller wing for its increased generating ability (explained in previous tests) and the lower cruise power. Both configurations use the larger mass and battery voltage following the trends shown in the previous tests.

The three optimized test results for the independent scenario are shown in Table 9. Though the wind power only result is still not be considered feasible due to the failure rate, the mission time has increased by a factor of 5 over the previous hybrid rotor optimizations while the failure rate has been cut in half. The combined power system also sees large improvements. The mission time increased by a factor of 1.6 while the failure time again decreased to half of the previous optimized designs.

Configuration	Best motor	Mission (%)	Failure (%)	Cruise power (W)	Generator power (W)
Wind	31	25.33	11.613	46.1	17.9
Combined power: large wing area	24	43.584	9.527	67.5	45
Combined power: small wing area	31	51.561	6.719	46.1	33.5

Table 9: Results of separate turbine optimizations without coordinating with the mothership.

Table 10 shows the results of similar tests but using the cooperating ship scenario. These results show the remarkable level of performance which may be possible if the source of updrafts can be improved. The cooperating ship scenario with only wind generation nearly tripled mission time of the optimized design from the same scenario while the combined configuration increased it by 50%. The tests were done with the ship assisting the aircraft when needed and these results showed the smallest amount of time making use of that assistance. All three tests result in zero failure time which is excellent.

Configuration	Best motor	Mission (%)	Cooperation with ship (%)	Cruise power (W)	Generator power (W)
Wind	28	48.756	17.61	46.1	25.1
Combined power: large wing area	27	57.743	16.48	67.5	53.3
Combined power: small wing area	28	66.172	13.38	46.1	39.7

Table 10: 0% failure results (by cooperating with the ship) for separate turbine optimizations.

Comparing the two results tables shows that significant gains can be made by improving the wind updrafts whether that be by altering the ship's heading or potentially some other method. A key effect is that using the ship to assist the aircraft trades ship control time for failure time but not at a 1:1 ratio. The failure rate is always less than the amount of time spent altering the ship's heading for the same design in the alternate scenario. This indicates that the ship is being utilized in situations where it is not needed to prevent failure. Ideally, the failure rate of the independent scenario should perfectly match the ship control time of the cooperative scenario to minimize the effect on the ship.

4 Discussion

This chapter begins with a more in-depth examination of the results presented in the previous chapter and how they relate to each other. After that are limitations of the model or control algorithms that were discovered in the results and suggestions to improve them. Lastly, there are several ideas which are considered that do not fully align with the research goals of this project but may better fulfill the mission requirements.

4.1 Deep dive in results

While each set of tests in the previous chapter provides information to improve those individual configurations, examining all of the results together reveals some additional interactions and information that can be used to form a more complete understanding of the project.

To answer the question of how well a propeller works as a turbine, it is best to directly compare the generating potential. Figure 23 shows a comparison between a turbine and a propeller of the same design for two wind speeds. Recall that positive values here represent turbine operation and negative values indicate propeller operation. Both have a diameter of 0.3556 m, pitch of 7 in, 2 blades, and zero extra twist. The physical difference in this case is which orientation the blade airfoil is in. The propeller has the top surface facing into the wind while the turbine has the bottom surface facing the incoming wind. The power figure on the left clearly shows at both wind speeds that the amount of power that can be generated is about two and a half times greater for the turbine orientation of the airfoil. You may also notice that the propeller has a negative power region for low tip speed ratios. The reason for this is that the 'incorrect' orientation has far greater drag at these conditions causing it to require additional power to cause it to spin. Because of this, roughly half of the potentially available tip speed ratios are unusable when trying to find a match in the soaring region. The turbine rotor does not have this problem and is capable of generating electricity at any slow rotational speed.

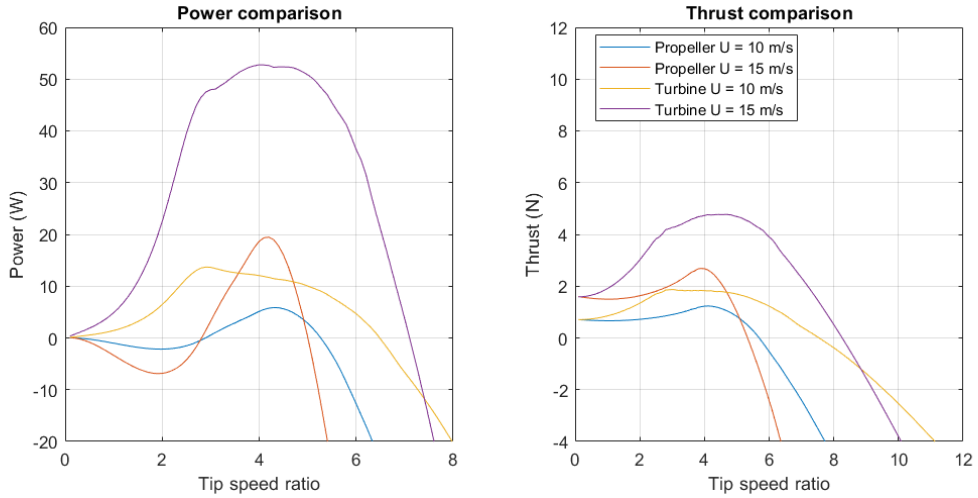

Figure 23: Comparison between turbine and propeller rotors of the same design except for the airfoil orientation, at two wind speeds.

Additionally, the thrust profile on the right of the figure is far better for generating electricity by having a larger range of rotor thrust values for one wind speed. A larger range means more flexibility in finding the correct operational state along with the potential for higher power operational states. When comparing the thrust of each rotor when operating as a propeller, the amount of power needed to produce a given thrust value appears to be roughly 2 times higher for the turbine rotor.

All of the rotor designs tested show similar results to these. All propellers have a large, negative-power region at low values for λ while the turbine versions of them do not have this limitation. The exact differences between the propellers and turbine versions of them do vary between the designs but always

show the same trend of significantly better generating potential but worse forward thrust potential for the turbines. This result is the inspiration for one of the additional ideas discussed in Section 4.3.

It is possible that with 2.5 times the generation at only twice the power cost, a wind turbine used as a propeller may have better results than a propeller used as a wind turbine. Much more investigation would be necessary for this conclusion however as these "turbine" designs are still based on the factors and design options of common airplane propellers. A properly designed and optimized wind turbine rotor may have significantly worse performance when pushing air like a propeller than this test shows.

Determining the most important characteristics for the motor/generator is another of the research goals of this project. The detailed tests of the two scenarios yielded some information but the separate turbine tests/optimizations gave a more complete picture. The separate turbine tests resulted in new motors/generators being used that were different from what were best for the hybrid rotor and solar aircraft tests. The new motors are number 28 which was never picked before, and 27 which was only used once in previous tests. This difference means it is worth examining the differences in what makes a good motor in each case. Each motor has three defining characteristics: kV, no-load current, and resistance. Figure 24 shows each of these characteristics plotted from lowest to highest with the few chosen best motors marked with color.

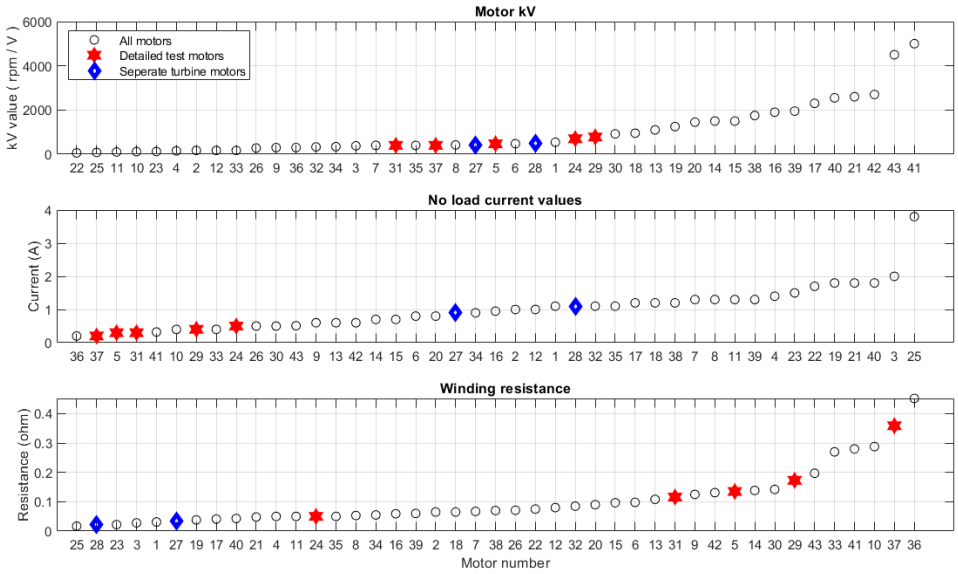

Figure 24: Plot showing all motor characteristics and marking all chosen (best) motors.

Each motor characteristic shows clear grouping indicating that the best motor (and desirable characteristics) can be predictable. All of the good motors have very similar kV ratings. Since kV is the relationship between angular velocity and voltage, it makes sense that all chosen motors would have nearly the same value because they operate at the same battery voltage and wind conditions. The no load current indicates a loss which scales with rotational speed. All motors, when used for thrust, must spin faster than the generating state so it makes sense that the best motors for the solar tests and hybrid rotor tests would prioritize a motor that is efficient while rotating quickly.

Separating the generator from the thrust motor allows the different needs of the generator to become visible. The best motors/generators for the separate turbine system prioritize a low resistance. This is likely because when generating electricity, the turbine spins slower than a motor would which, by the relationship in Equation 25 and ohm's law, would lead to high current and thus high resistive losses. Similarly, with a generally slower turning rotor, the no load current would be less important which is also clearly shown in the middle plot of the figure.

Examining the relationship between the rotor design and the potential soaring region calculated by the wind field program shows that the updraft energy is underutilized. All tested cases produce 'match

plots' like Figure 18 where the potential states reach the upper limit line and sometimes reach the lower limit. One additional match test is shown in Figure 25 where a rotor with a much larger diameter was used to test the higher limits of the matching system. A much larger diameter would be capable of generating more power and applying more drag than any of the tested designs. As shown in the figure, the match points do not reach the power line for the maximum wind speed indicating that this rotor has exceeded the maximum allowable drag calculated by the wind field program but still has a range of lower drag values capable of finding matches. In this case, the rotor is underutilized rather than the updraft.

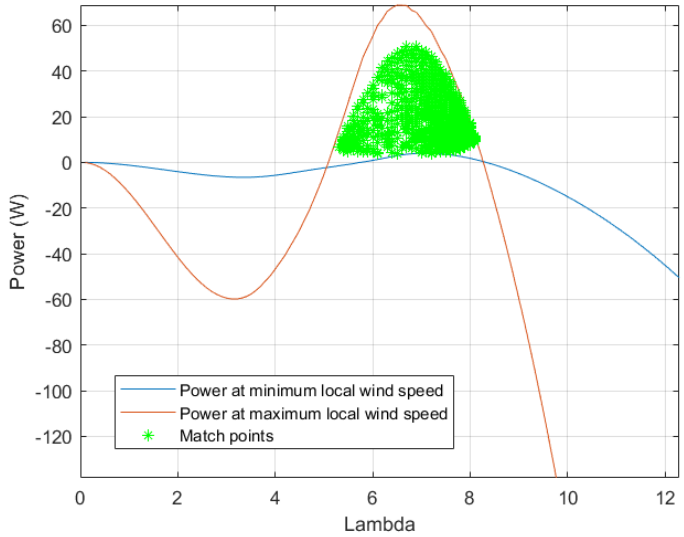

Figure 25: Plot showing potential operating points at 10 m/s for 1 meter diameter oversized rotor.

To understand what happened it is useful to have a deeper explanation of how the wind field program calculates the available drag in the soaring region. An additional input to this program is rotor area which informs the program what the maximum amount of drag that can be applied is. This is done using an ideal rotor which is certainly not going to match the rotors tested in this report. So, for the purposes of this project, the rotor area input was neglected as a variable and replaced with an exceptionally high value of 2 m^2. The fact that a 1 m diameter simulated rotor was able to exceed the drag allowed by an ideal rotor (as shown in the figure) that is noticeably larger, is proof that using a much larger value for rotor area in the wind field program was a good decision. Doing so allowed the matching algorithm to find all potential operational states unimpeded by the limitations of a simple ideal rotor.

Further increases to the rotor area in the wind field program would further increase the available drag but not without limit. An increase to this rotor area does not affect the calculations of the soaring region for smaller rotors, it simply extends the region in the direction of higher drag and thus power. This region can be seen in Figure 13 as getting closer to the front of the ship and lower in elevation (z position). However, as shown by the match plots Figure 18 and Figure 25, increasing the size and max drag of the soaring region was unnecessary because none of the planned tests were capable of reaching the maximum allowable drag. This means that even the separate turbine tests were unable to fully utilize the available power and larger rotors or multi-rotor systems could be explored.

4.2 Improvements to flight control and future research

The model, flight controller, and simulations used in this report had many simplifications and limitations. This part of the report will point them out and offer suggestions for improvement and also areas where more research is needed.

The first limitation to discuss is the very simple flight controller used to direct the aircraft in the

simulations. Every simulation used the same algorithm with only slight differences made between the different generation methods. One undesirable effect of the algorithm is shown most clearly by some solar aircraft runs. Cases where the aircraft had a greater amount of power required for cruise flight would have reduced failure rates. This occurred because the desired charge remaining when returning from being on mission was a function of the cruise power when it should have been a function of the power needed while soaring. All designs used the same amount of power while soaring so the amount of time the aircraft could soar without charging changed with the power needed for cruise flight.

To improve this part of the algorithm, a constant value of Watt-hours should be reserved for soaring at the ship. This would solve the issue. Further improving the simulation, the safety margin could also become a design variable to find out how much reserve power would produce the best mission time and lowest failure rate. Or perhaps it would be possible to make a better prediction for how much energy should be reserved to last until the next charging opportunity.

Another unintended effect of soaring happens to the hybrid rotor aircraft and can be seen in Figure 21 and Figure 26 (particularly at 1.06 on the x-axis). Here, the aircraft is soaring but still expending net energy resulting in the eventual drain of the battery. Once that happens there is a single time step registering a failure state but since the aircraft is still capable of soaring it is immediately re-launched with a small charge. In early versions of the model, a failure state would fully re-charge the battery before launching which resulted in an artificially high mission time. Altering the model to give the aircraft only a very small charge reduced this issue but as shown in the figures, it is still artificially reducing the failure rate by giving the aircraft enough charge to finish the low-energy period.

Two things could fix this issue. Increasing the reserve power and setting it as a constant or design variable would prevent failure during these situations. Alternatively, adjusting the flight controller to make better decisions for when it is safe to re-launch the aircraft would prevent the artificial reduction in failure rate.

Another note is that the occurrence of "failure" is unrealistic. In reality, if the aircraft runs out of energy then it will be destroyed in the sea; there is no recovery and relaunch option. Relaunching the aircraft in the simulation is just a way to continue running the simulation which is why it is important that the conditions of the relaunch not alter the results.

A third improvement to the model during soaring could be partial-power soaring for the independent ship scenario. The program from the other researcher which produces the stable soaring region could include an expanded area where part of the aircraft lift comes from the updraft while the rest is supplemented by expending energy with the propeller. This would significantly reduce failure rates in cases such as what is shown in Figure 26. In this case, the aircraft has a very high cruise power and any time the wind speed dips slightly below the minimum speed that allows static soaring, the aircraft immediately switches to full powered flight which drains the battery very quickly resulting in failure. This can most easily be seen on the second peak of the battery status plot where the SOC drops slowly while soaring until the wind speed drops causing the SOC to plummet. The issue of low wind speed is almost entirely fixed in the scenario where the ship assists in low wind situations.

An alternative solution which requires less work is to simply reduce the cruise speed. In the simulation the aircraft is assumed to always be moving at cruise speed when not soaring. What may make the difference for the simulated aircraft is if the aircraft only needed to match the airspeed of the ship. Reducing the flight speed reduces the power needed by the motor. By reducing the amount of power needed when the aircraft are not on mission but unable to soar at the ship, they may have had enough energy to last until the next charging opportunity. This would not help in all cases as often the aircraft may need to wait for several hours before it can charge again. In Figure 26 however, there are several instances where there was only a short failure interval before the next charging opportunity appeared.

On the subject of the ship, the percent of time that the ship is controlled by each design is typically in the 30% range. Any value below 50% means that the ship is probably capable of eventually reaching an intended destination but a lower value of impact is always better. Any time a greater updraft is needed, the ship turns directly into the wind but if the ship turned only partially into the wind to

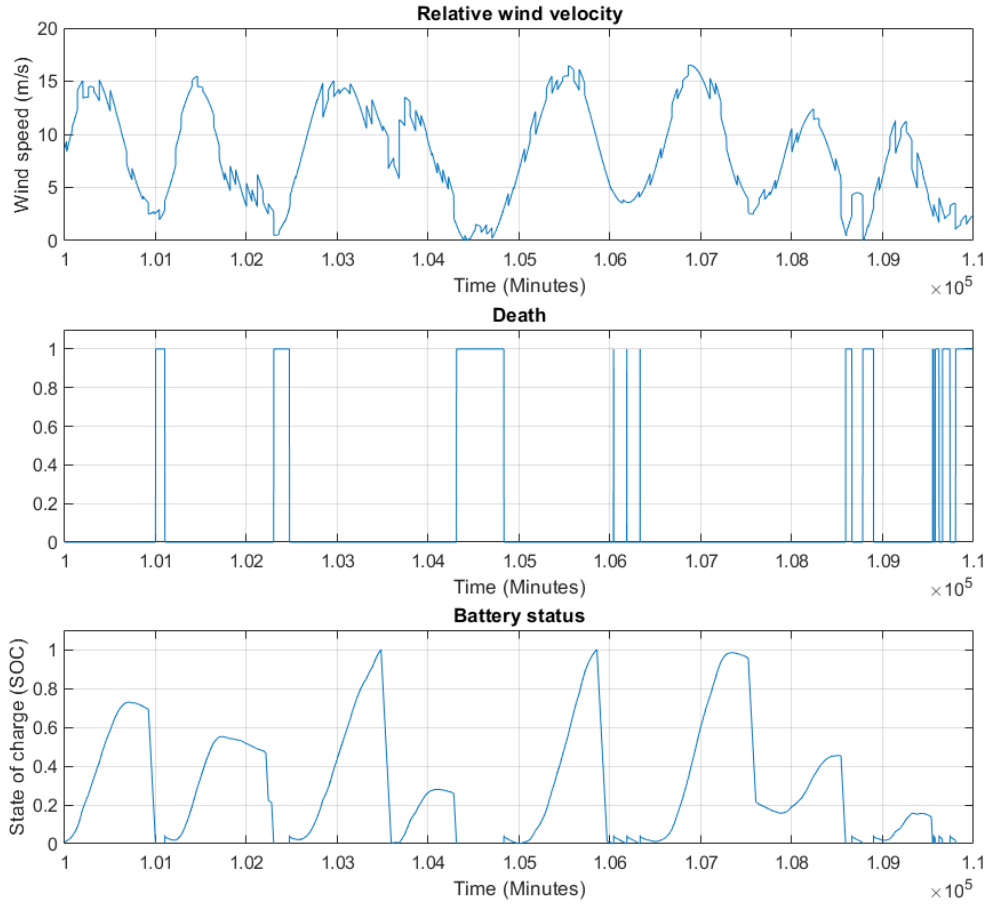

Figure 26: Failure of high cruise power design shows several instances of re-launching when conditions are not good resulting in additional failures.

increase the relative wind speed only by the amount needed could decrease the effect on the ship's own mission. Two problems exist with this idea though. If the ship is not maximizing the wind speed for the aircraft then it is possible that it may be stuck on an undesirable heading without charging the aircraft very quickly resulting in an overall increase in the time that the ship is affected.

The second issue is one that actually already is part of the project: the effect of soaring at an angle to the relative wind. This was not included in the soaring program from the other researcher so its effect is unknown. The unknown effects of an off-center wind and the accompanying complicated issue of controlling the aircraft within the wind field are the two largest factors which could reduce the effectiveness of the hybrid rotor and uplift ideas. Exploring these issues are already current or future parts of the larger project with the MAVLab.

Back to the subject of improving the simulation results, there is another change that should be made to the flight algorithm. The solar aircraft is capable of charging in flight and in many situations, such as what is shown in Figure 21, the solar aircraft achieves full charge through the middle of the day. This is all wasted energy which could be used to increase mission time. Altering the controller to send the aircraft on mission before it is fully charged or even before the net charge is increasing would increase the amount of solar energy that can be collected (by expending more) and thus increase total mission time. To do this, a fairly accurate prediction of the weather for the full day would be required and a mistake in the prediction could result in a drained battery and failure of the aircraft. Alternatively, larger batteries could be used to smooth out the differences in solar output across multiple days rather than the current system of fully charging and discharging the battery every day. utilizing this extra energy with a larger battery could extend night operations or decrease the failure rate from random bad conditions.

Adjustments to the aircraft design could also improve the accuracy of the model or increase the effectiveness that it predicts. No changes were made to the airfoil of the blade or the airfoil of the wing for the tests in this report, however some evidence was shown that implies improvements could be made in this area when choosing the design of the airframe or custom rotor. Figure 8 is a comparison of the performance of the chosen blade airfoil in two orientations and a randomly chosen symmetrical airfoil. This figure shows that the generation performance is close to that of the properly oriented turbine blades and the propeller performance is not significantly worse than the original propeller design. A single test has been performed to compare the performance of this symmetric airfoil for the hybrid rotor configuration in the independent scenario with the rotor design of the first row of Table 5. The results of this comparison are shown in Table 11 which support what was expected. It doubles the energy generation over the NACA 4412 airfoil used in all of the other tests while only increasing the power consumption in cruise by 17%. The symmetric airfoil more than triples the mission time and decreases the failure time by a small amount. If custom rotors are the future of this project, then symmetric airfoils must be examined further.

	NACA 4412	ea 61012
Mission time (%)	1.81	6.83
Failure time (%)	24.2	22.6
Motor number	24	31
Mean charge rate (W)	8.2	16.2
Cruise Power (W)	92.3	108.6

Table 11: Results of original design first case compared to symmetric airfoil test of the same design.

Another airfoil which can be adjusted is the airfoil used for the aircraft's wings. As explained in the results section, the chosen airfoil (MH32) produces too much lift and as a result causes excess drag. Additionally, the turbine aircraft functions better with smaller wings that produce less lift as that permits it to apply more drag and generate more electricity. Both of these factors indicate that using a high-lift competition glider airfoil may be the wrong choice for this use case. An airfoil that produces only as much lift as needed and can operate with less drag would reduce the cruise power in all cases

and improve the turbine generation performance. The amount of difference is unknown and requires further research.

4.3 New ideas

Doing this project has resulted in a few creative ways to significantly improve performance of the aircraft in its mission which do not quite match well enough with the project goals to explore explicitly. One idea is an improvement to the solar-type aircraft from Bart Remes of the MAVLab while the other is the author's idea to improve the turbine-powered plane.

Beginning with the solar idea, a focused light source mounted to a gimbal on the ship could be used to charge the aircraft via an underside solar panel. By doing this it would eliminate any need to use static soaring and reduce dependence on the solar cycle. Continuing to have solar panels on the tops of the wings would be unnecessary but would still increase daytime activity. This could allow a greater variety of missions including night time operation. It would also entirely eliminate the possibility of the aircraft running out of power so long as the weather and wind direction is monitored so that the aircraft can return to the ship. This would be a truly never-landing drone and it could be done in two main ways.

The simplest way is to have a large generic solar panel area on the bottom of the aircraft and a powerful but otherwise unremarkable spotlight on the ship. This light would require significant power and/or focus as the available energy supplied to the aircraft would decrease with the square of distance and the aircraft would likely have a thin and wide target area (the wing) requiring accuracy or a much larger and stronger beam. This transfer would also be limited by the efficiency of solar panels which could be further reduced depending on the suitability of the spotlight spectrum. Additionally, if this aircraft is used by the navy for surveillance then they may have some level of reluctance about displaying their location with a skyward spotlight.

An alternative is to exploit the nature of the photovoltaic effect and have a more expensive but better, more tuned system. A solar panel must receive photons of a certain energy to produce any electricity at all. However, any energy higher than this level is wasted as heat. For sunlight on a silicon solar panel, some of the energy is unusable and the rest is underutilized resulting in an efficiency of 20%. The wavelength of light that is needed for silicon cells is 1107 nm [23] which is in the invisible infra-red region of the electro-magnetic spectrum. Figure 27 shows the External Quantum Efficiency (EQE) for a silicon solar cell. This value represents the ability of a solar cell to absorb and convert a photon of particular wavelength into electricity. Knowing that the energy of a photon in inversely proportional to its wavelength, an optimal wavelength can be calculated. A few percent of additional losses must be added on top such as electrical resistance and reflections [23].

Based on Figure 27, a laser that can produce a beam at the ideal wavelength (near 1000 nm), which is readily available [26], would be able to achieve an estimated transfer efficiency in the range of 80% on a much smaller target area. Exploring other solar cell types may further improve the efficiency. A reduction in the amount of wasted energy and improved focus could reduce the amount of heat energy absorbed by the aircraft by an order of magnitude when compared to a spotlight. For high speed charging of the aircraft, a more precise light emitter would reduce the possibility of excess heat damaging systems or melting the airframe. The invisible beam may also suit the needs of the navy better. An arbitrarily high charge rate of 1 kW, which is 5x the peak charge rate of any of the solar aircraft tests in this report, should not be difficult in this case.

The other idea is to use a variable pitch rotor hub and zero pitch blades to improve the thrust and generating capabilities of the hybrid rotor. This concept is not part of the project by default because it involves adding a very complex mechanism to the rotor hub requiring additional control and actuators. The practical effect of this device would be to rotate the blades of the rotor by 180 degrees so that, with the motor spinning in the opposite direction, the rotor airfoils could operate efficiently both when producing forward thrust and producing electricity. This is similar to the separate turbine tests except that the propeller and turbine would have the same diameter and blade number but they would have

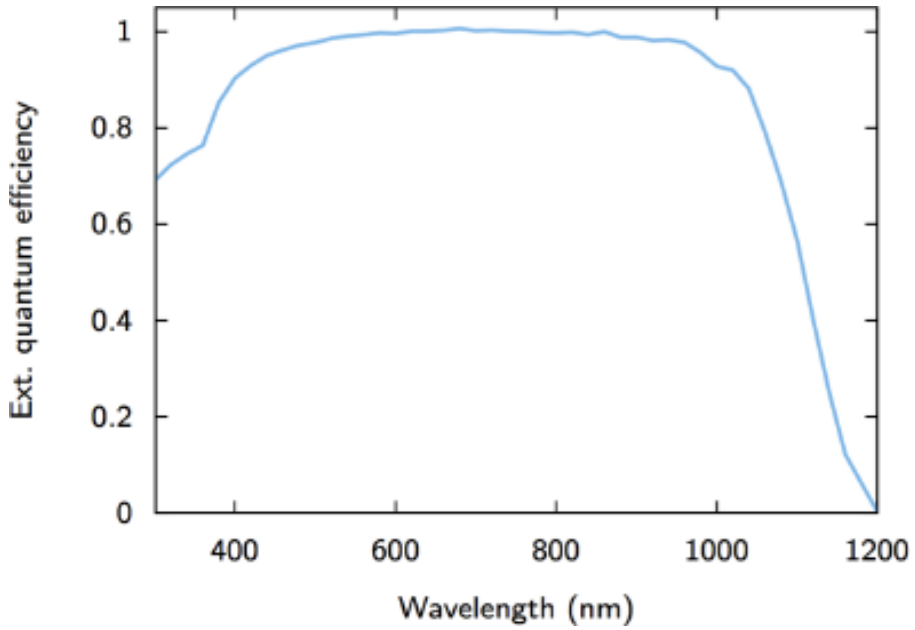

Figure 27: External quantum efficiency of quality silicon [23].

to use blades with no pitch. Additionally, with a more complex controller, the "extra twist" could be varied in-flight to maximize performance in the widely varying generating conditions.

When comparing the separate turbine tests to the static hybrid propeller we can see how much of a difference the airfoil orientation makes in generating potential. All the same design variables are used between the two sets of tests with the primary difference being the orientation of the airfoil. One comparison can be directly made based on the data already produced from the tests in Section 3. The rotor design most efficient in cruise has the default values but with pitch changed to 10 inches. Unfortunately, on the hybrid rotor aircraft it only produces 0.2% mission time. The same design in the separate turbine tests results in 8.2% mission time which is factor of 40x better. This would be similar to the difference that could be achieved with this rotor design and a rotor hub that is capable or rotating the blades completely around on command.

5 Conclusion and Recommendation

Reviewing all of the results shows a few key points of information. The initial vision of the project was to design an aircraft which could statically soar around a naval ship indefinitely by recharging itself in the updrafts (caused by the ship) with its propeller using no additional components. This is likely not possible due to overall heavy reliance on variable wind conditions and low generating potential of such a small and poorly optimized "wind turbine". All of the tests for this idea were barely able to generate enough power to operate the on board electronics. The completely opposite design approaches to wind turbines and propellers is a problem that cannot be ignored. Using a normal propeller as a wind turbine is not feasible on its own. Without some other method of improving the wind conditions at the ship, ordering it to deviate from its course to assist the aircraft will be necessary or the aircraft will fail the mission. However, with creative alternatives, failure rates have been decreased to single digit percentages of time.

When designing the NLD system, several lessons have been learned through the course of this project. The design approach of the rotor is almost exactly opposite between propellers and wind turbines. This includes the airfoil orientation, rotor size, and pitch of the rotor. The motor also has differing requirements further leading to the unsuitability of the combined approach. Wind turbines tested in this report spin more slowly and thusly prefer motors/generators with better low voltage/high current performance whereas the propeller prefers a motor efficient at higher RPM. This is the main limitation of the hybrid rotor aircraft when compared to the solar configuration.

A few more important lessons were learned about the design of the airframe and common systems. The solar configuration saw minimal improvement from a larger solar collector area due to the increased drag of the larger wing but a more detailed design and optimization of the wings including their airfoil could fix this in future research. The potential wind energy is inversely related to the wing area indicating that when generating power while soaring, it is preferable to "catch the wind" with the turbine more than with the wings. Lastly, the battery cell count does not matter in a high-level analysis such as this so other factors will have to drive that decision.

The alternate possibilities that were also analyzed including the addition of solar power, changing the ship's course to maximize wind, and a separate more efficient turbine, do not perfectly meet the design goals of the project but are able to complete the desired mission with greater effectiveness and success. With respect to the mission time, all cases showed that the purely solar powered aircraft performed better than the hybrid rotor aircraft by a significant margin indicating that it is clearly the better choice from a pure utility standpoint. However, it often had greater failure rates due to a heavy dependence on seasonal sunshine making it unsuitable for unending flight with the current design limitations. Combining the hybrid rotor concept and solar generation results in a significant synergistic effect which improves mission performance but still suffers from a high failure rate when operating independently of the ship.

Adjusting the heading of the ship to maximize wind updrafts is able to almost completely remove any instances of aircraft failure in all cases and can reach significant amounts of mission time, but is a major compromise on the goal of operating independently of the mothership. Improvements to the flight algorithm, as was described in Section 4.2, could certainly remove the last fractions of percent of failure time in this scenario regardless of the chosen power source. When cooperating with the ship, a mission-to-charge-time ratio of 1:6 is possible for the hybrid rotor aircraft, 3:7 for the solar aircraft and up to 2:3 when using both wind and solar energy.

The best choice for the future of this project is to include one of the two turbine ideas mentioned in this report. A rotor hub capable of twisting the blades around would certainly improve performance but would still be held back by some of the conflicting needs of a propeller and wind turbine (blade twist profile). Having a separate motor and optimized wind turbine and including solar panels is a configuration capable of achieving incredible mission-to-charge-time ratios of 2:1 when being actively assisted by the mothership or 1:1 with no active assistance from the ship while having a failure rate of only 7%. Improvements to the control of the aircraft and how it manages its charging periods and

improvements to how the simulation handles these situations would improve this design beyond its current level of performance and may even make it possible to eliminate the failure rate entirely to make a truly never landing drone.

Bibliography

[1] Nangia R. K. "operations and aircraft design towards greener civil aviation using air-to-air refueling". In: *The Aeronautical Journal* (2006), pp. 1–14. URL: https://web.archive.org/web/20131021064242/http://www.greenerbydesign.org.uk/_FILES/publications/3088.pdf.

[2] Milko Vuille. *Solar Impulse SI2 pilote Bertrand Piccard Payerne November 2014.jpg*. Nov. 13, 2016. URL: https://en.wikipedia.org/wiki/File:Solar_Impulse_SI2_pilote_Bertrand_Piccard_Payerne_November_2014.jpg.

[3] *Ridge/Slope Soaring (Part One)*. Fight Literacy. URL: https://www.flightliteracy.com/ridge-slope-soaring-part-one/ (visited on 04/08/2021).

[4] Phillip L. Richardson, ed. *High-Speed Dynamic Soaring* (Apr. 2012): *R/C Soaring Digest*.

[5] Pranay Sinha Damon Vander Lind. "Motor pylons for a kite and airborne power generation system using same". US 8,955,795 B2. Feb. 17, 2015.

[6] Corwin Hardham Damon Vander Lind Beekar Van Niekerk. "Tethered system for power generation". US 2010/0295303 A1. Nov. 25, 2010.

[7] *13 years of Makani airborne wind energy knowledge available open source*. TU Delft. Oct. 9, 2020. URL: https://www.tudelft.nl/en/2020/lr/13-years-of-makani-airborne-wind-energy-knowledge-available-open-source (visited on 04/08/2021).

[8] A Gambardella T Huld R Müller. "A new solar radiation database for estimating PV performance in Europe and Africa". In: *Solar Energy* 86 (6 2012), pp. 1803–1815.

[9] M. K. Rwigema. "Propeller blade element momentum theory with vortex wake deflection". In: International congress of the aeronautical sciences. Vol. 27. 2006.

[10] R. E. Wilson. "Wind-turbine aerodynamics". In: *Journal of Industrial Aerodynamics* (1980).

[11] Axelle Viré Michiel Zaaijer. "Introduction to wind turbines: physics and technology". In: (Nov. 10, 2018).

[12] *Engineering Design Process Used to Develop APC Propellers*. Landing Products Inc. URL: https://www.apcprop.com/technical-information/engineering/ (visited on 04/08/2021).

[13] Midas Gosye. "Study on the feasibility on using a combination of static, orthographic, and regenerative soaring to achieve unlimited endurance for UAVs". thesis. Technical University Delft, 2021.

[14] *Airfoil database search*. Airfoil Tools. URL: http://airfoiltools.com/search/index (visited on 04/08/2021).

[15] *Brushless Motor Efficiency and Constants*. Radio Control Info. URL: https://www.radiocontrolinfo.com/brushless-motor-efficiency/ (visited on 04/08/2021).

[16] Adam Tomaszuk and Adam Krupa. "High efficiency high step-up DC/DC converters - A review". In: *Bulletin of the Polish Academy of Sciences: Technical Sciences* 59 (Dec. 2011). DOI: 10.2478/v10175-011-0059-1.

[17] Clayton R. Green. "Modeling and test of the efficiency of electronic speed controllers for brushless dc motors". thesis. California Polytechnic State University, Sept. 2015.

[18] *Guardian*. Netherlands Coastguard. URL: https://www.kustwacht.nl/en/node/206 (visited on 04/09/2021).

[19] *Hourly data of the weather in the Netherlands*. Royal Netherlands Meteorological Institute. Potential wind station 252, 2011.

[20] *Victor F3J/F3B*. ICARE Sailplanes and Ekectrics. URL: http://www.icare-rc.com/victor.htm (visited on 04/08/2021).

[21] Reto Foilka. "F3B – the optimization of different flying states". In: *Modell Flugsport* (2007).

[22] *Overview of Lithium Ion batteries*. Panasonic. 2007.

[23] et al. Arno Smets Klaus jager. *Solar Energy: The physics and engineering of photovoltaic conversion, technologies and systems*. UIT Cambridge Limited, 2016. ISBN: 978-1-906860-32-5.

[24] Talu B Wata J Faizal M. *Studies on a low Reynolds number airfoil for small wind turbine applications*. report. University of the South Pacific, 2011.

[25] Paul C.Kilmes Robert E. Sheldahl. *aerodynamic characteristics of seven symmetrical airfoil sections through 180-degree angle of attack for use in aerodynamic analysis of vertical-axis wind turbines*. report. Sandia national Laboratories, 1981.

[26] *Single Mode Rackmount Fiber Lasers*. nLIGHT. 2019. URL: https://static1.squarespace.com/static/5d5d8be5c16a590001b58605/t/5e45fe12ebee3761588bbd58/1581645331690/nLIGHT_DS_500_1200W_Single+mode_JUNE_2019_FNL2.pdf.

[27] *T-Motor*. 2020. URL: https://uav-en.tmotor.com/.

[28] *Cobra Motors*. Danlions Electric Industrial Co., Ltd. 2020. URL: https://www.cobramotorsusa.com/about.html.

A Appendix: Motor specifications table

Motor Number	kV	i_o	R_{motor}
1	540	1.1	0.031
2	170	1	0.065
3	380	2	0.028
4	150	1.4	0.05
5	470	0.3	0.135
6	475	0.8	0.098
7	400	1.3	0.067
8	420	1.3	0.053
9	300	0.6	0.125
10	115	0.4	0.288
11	100	1.3	0.05
12	170	1	0.08
13	1100	0.6	0.108
14	1500	0.7	0.1385
15	1500	0.7	0.0965
16	1900	0.95	0.059
17	2300	1.2	0.041
18	950	1.2	0.065
19	1250	1.8	0.038
20	1450	0.8	0.09
21	2600	1.8	0.048
22	60	1.7	0.075

Motor Number	kV	i_o	R_{motor}
23	120	1.5	0.022
24	700	0.5	0.05
25	80	3.8	0.017
26	280	0.5	0.071
27	420	0.9	0.033
28	490	1.1	0.021
29	780	0.4	0.173
30	920	0.5	0.142
31	400	0.3	0.116
32	330	1.1	0.085
33	170	0.4	0.27
34	340	0.9	0.055
35	400	1.1	0.05
36	300	0.2	0.452
37	400	0.2	0.359
38	1750	1.2	0.07
39	1950	1.3	0.06
40	2550	1.8	0.043
41	5000	0.32	0.28
42	2700	0.6	0.131
43	4500	0.51	0.197

Table 12: Values of the three motor parameters used for all motors. These values come from the manufacturers T-Motor and cobra Motors.[27] [28]